The Astrophysical Journal, 767:120 (20pp), 2013 April 20 doi:10.1088/0004-637X/767/2/120
© 2013. The American Astronomical Society. All rights reserved. Printed in the U.S.A.

A WFC3/*HST* VIEW OF THE THREE STELLAR POPULATIONS IN THE GLOBULAR CLUSTER NGC 6752*

A. P. Milone[1,2,3], A. F. Marino[1,4], G. Piotto[5,6], L. R. Bedin[6], J. Anderson[7], A. Aparicio[2,3], A. Bellini[7], S. Cassisi[8], F. D'Antona[9], F. Grundahl[10], M. Monelli[2,3], and D. Yong[1]

[1] Research School of Astronomy and Astrophysics, The Australian National University, Cotter Road, Weston, ACT, 2611, Australia; milone@mso.anu.edu.au, amarino@mso.anu.edu.au, david.yong@anu.edu.au
[2] Instituto de Astrofísica de Canarias, E-38200 La Laguna, Tenerife, Canary Islands, Spain; aparicio@iac.es, monelli@iac.es
[3] Department of Astrophysics, University of La Laguna, E-38200 La Laguna, Tenerife, Canary Islands, Spain
[4] Max Planck Institute for Astrophysics, Postfach 1317, D-85741 Garching, Germany
[5] Dipartimento di Astronomia, Università di Padova, Vicolo dell'Osservatorio 3, Padova I-35122, Italy; giampaolo.piotto@unipd.it
[6] INAF-Osservatorio Astronomico di Padova, Vicolo dell'Osservatorio 5, I-35122 Padua, Italy; luigi.bedin@oapd.inaf.it
[7] Space Telescope Science Institute, 3800 San Martin Drive, Baltimore, MD 21218, USA; jayander@stsci.edu, bellini@stsci.edu
[8] INAF-Osservatorio Astronomico di Collurania, via Mentore Maggini, I-64100 Teramo, Italy; cassisi@oa-teramo.inaf.it
[9] INAF-Osservatorio Astronomico di Roma, Via Frascati 33, I-00040 Monte Porzio Catone, Rome, Italy; dantona@mporzio.astro.it
[10] Department of Physics and Astronomy, Arhus University, Ny Munkegade, DK-8000, Arhus C, Denmark; fgj@phys.au.dk
Received 2012 October 4; accepted 2013 January 28; published 2013 April 4

ABSTRACT

Multi-band *Hubble Space Telescope* photometry reveals that the main sequence, sub-giant, and the red-giant branch of the globular cluster NGC 6752 splits into three main components in close analogy with the three distinct segments along its horizontal branch stars. These triple sequences are consistent with three stellar groups: a stellar population with a chemical composition similar to field-halo stars (Population a), a Population (c) with enhanced sodium and nitrogen, depleted carbon and oxygen, and an enhanced helium abundance ($\Delta Y \sim 0.03$), and a Population (b) with an intermediate (between Populations a and c) chemical composition and slightly enhanced helium ($\Delta Y \sim 0.01$). These components contain ∼25% (Population a), ∼45% (Population b), and ∼30% (Population c) of the stars. No radial gradient for the relative numbers of the three populations has been identified out to about 2.5 half-mass radii.

Key words: globular clusters: individual (NGC 6752) – stars: Population II

Online-only material: color figures

1. INTRODUCTION

It is now widely accepted that many (if not all) globular clusters (GCs) are made up of multiple populations of stars. Since the 1970s, it has been well known that stars within the same cluster have light-element abundance variations (e.g., Kraft 1979; Norris & Freeman 1979), but at that time it was not clear whether these "abundance anomalies" were due to internal mixing or differences in the primordial composition or a combination of these effects. More recently, high-resolution spectroscopy has revealed the presence of well-defined correlations among some light-element abundances (e.g., Kraft et al. 1992; Sneden et al. 1994; Ramírez & Cohen 2002), including the anticorrelations between Na and O, and Mg and Al, which indicate that material has been processed via high-temperature proton capture nucleosynthesis (Denisenkov & Denisenkova 1989).

The fact that the same light-element variations have also been observed in unevolved cluster stars (e.g., Briley et al. 1994, Briley 1997; Cannon et al. 1998; Gratton et al. 2001), whose internal temperatures do not allow high-T proton captures, and in fully convective low-mass M-dwarfs (Milone et al. 2012d) suggests that these stars were born with these chemical peculiarities imprinted in the matter from which they formed (Cottrell & Da Costa 1981, see Gratton et al. 2004 for a review).

High-precision *Hubble Space Telescope* (*HST*) and ground-based photometry has shown that several GCs host multiple main sequences (MSs), including ω Centauri, NGC 2808, 47 Tuc, NGC 6752, and NGC 6397 (Anderson 1997; Bedin et al. 2004; Piotto et al. 2007; Milone et al. 2010, 2012a, 2012b), which have been associated with stellar populations with different helium abundances (D'Antona & Caloi 2004; Norris 2004; Bedin et al. 2004; Piotto et al. 2005; D'Antona et al. 2005). Multiple stellar populations have also been detected in the color–magnitude diagram (CMD) from the presence of multiple sub-giant branches (SGBs; Milone et al. 2008; Anderson et al. 2009; Marino et al. 2012; Piotto et al. 2012) or multiple or spread red-giant branches (RGBs; e.g., Grundahl et al. 1998, 2000; Yong et al. 2008; Marino et al. 2008; Lee et al. 2009).

Stellar evolution models predict that high-temperature H-burning through the CNO cycle should result in an increase of the N abundance, at the expenses of C and O, and of an increase in the helium fraction. Multiple stellar populations with different helium contents could also account for the horizontal branch (HB) morphology of some GCs in which the bluer HB sequences can be associated with the presence of He-rich stars (e.g., D'Antona et al. 2002; D'Antona & Caloi 2008; Busso et al. 2007; Cassisi et al. 2009; Catelan et al. 2010; Dalessandro et al. 2011). Indeed, clear evidence of the connection between the HB morphology with the multiple populations comes from Marino et al. (2011), who have found that blue-HB stars of the GC M 4 are all Na-rich and O-poor (hence He-rich), whereas red-HB stars are primarily Na-poor and O-rich (He-poor; see also Norris 1981; Smith & Norris 1993). Similar results have been found in NGC 2808 (Gratton et al. 2011).

This work adds yet another cluster (NGC 6752) to the growing list of clusters with photometric and spectroscopic evidence of multiple sequences along the RGB, MS, SGB, and HB. We use *HST* filters covering a wide range of wavelengths to study the multiple stellar populations in the GC NGC 6752. The presence

* Based on observations with the NASA/ESA *Hubble Space Telescope*, obtained at the Space Telescope Science Institute, which is operated by AURA, Inc., under NASA contract NAS 5-26555.

Table 1
Description of the *HST* Data Sets used in this Paper

Instr	Date	$N\times$exptime	Filter	Program	PI
WFC3/UVIS	2010 Aug 21	6 × 120 s	F225W	11904	Kalirai
WFC3/UVIS	2011 Mar 23, Apr 3	12 × 360	F275W	12311	Piotto
WFC3/UVIS	2010 May 5	30 s + 2 × 500 s	F336W	11729	Holtzman
WFC3/UVIS	2010 May 5	2 × 2 s + 2 × 348 s+ + 2 × 880 s	F390W	11664	Brown
WFC3/UVIS	2010 May 5	50 s + 2 × 700 s	F390M	11729	Holtzman
WFC3/UVIS	2010 May 5	90 s + 2 × 1050 s	F395N	11729	Holtzman
WFC3/UVIS	2010 May 5	40 s + 2 × 800 s	F410M	11729	Holtzman
WFC3/UVIS	2010 May 5	40 s + 2 × 400 s	F467M	11729	Holtzman
WFC3/UVIS	2010 Aug 7, 21	12 × 670 s	F502N	11904	Kalirai
WFC3/UVIS	2010 May 5	5 s + 40 s + 400 s	F547M	11729	Holtzman
WFC3/UVIS	2010 Jul 31, Aug 7, 21	15 × 550 s	F555W	11904	Kalirai
WFC3/UVIS	2010 May 1	30 s + 2 × 665 s	F555W	11664	Brown
WFC3/UVIS	2010 Jul 31, Aug 7, 21	15 × 550 s	F814W	11904	Kalirai
WFC3/UVIS	2010 May 1	30 s + 2 × 495 s	F814W	11664	Brown
WFC3/UVIS	2011 Mar 23, Apr 3	2 × 50	F814W	12311	Piotto
WFC3/NIR	2010 May 1	3 × 4 s + 3 × 49 s + 299 s + 2 × 399 s	F110W	11664	Brown
WFC3/NIR	2010 May 1	3 × 4 s + 3 × 49 s + 299 s + 2 × 399 s	F160W	11664	Brown
ACS/WFC	2006 May 24	1 × 2 s + 4 × 35 s	F606W	10775	Sarajedini
ACS/WFC	2006 May 24	1 × 2 s + 4 × 40 s	F814W	10775	Sarajedini

of star-to-star light-element variations in the cluster has been widely reported in the literature (Norris et al. 1981; Grundahl et al. 2002; Yong et al. 2003, 2005, 2008; Carretta et al. 2007).

Photometric evidence for three populations of stars along the RGB of NGC 6752 with different Mg, Al, Mg, Si, Na, and O contents was identified early by Grundahl et al. (2002) and Yong et al. (2008, see also Carretta et al. 2012). These authors found that the Strömgren photometric index c_1 correlates with nitrogen abundance in stars both brighter and fainter than the RGB bump, and suggest that the observed photometric scatter is due to stellar populations with different N abundance (see also Milone et al. 2010; Kravtsov et al. 2011; Sbordone et al. 2011).

The HB of NGC 6752 also revealed a complex structure with two discontinuities that define three HB segments (Momany et al. 2002, 2004). Villanova et al. (2009) analyzed the spectra of seven HB stars with effective temperature $\sim 8000 < T_{\rm eff} < 9000$ K and found that six of them have a chemical composition similar to field-halo stars, including helium. A recent photometric analysis of data collected with the Advanced Camera for Survey (ACS) on board *HST* also showed that NGC 6752 has a broadened MS with some indication of an MS split (Milone et al. 2010), thus suggesting that its stellar populations also have different helium contents.

The paper is organized as follows. In Section 2, we present the data and describe the data reduction. In Sections 3, 4, and 5, we study the triple MS, SGB, and RGB, respectively. An effort was made to disentangle the multiple populations in each of these three evolutionary sequences separately. In Section 6, we explore possible theoretical interpretations and estimate the helium difference among the three stellar populations. The study of the radial distributions of the various stellar populations is also undertaken. Finally, a summary and some discussion follow in Section 7.

2. OBSERVATIONS AND DATA REDUCTION

This work makes use *of* two data sets. For the central regions of the cluster, we used both archival and proprietary material collected with the UV–visual (UVIS) and infrared (IR) channels of the Wide Field Camera 3 (WFC3), and the wide-field channel (WFC) of the ACS mounted at the *HST*. Proprietary images (under program GO-12311, PI: Piotto) were collected in two one-orbit visits taken at two different orientations, the first one on March 23, and the second one on 2011 April 3, and consist of 12 × 360 s images in camera/channel/filter WFC3/UVIS/F275W, and 2 × 50 s in WFC3/UVIS/F814W. We also used the photometric catalogs presented by Anderson et al. (2008) and obtained from ACS/WFC images taken under GO-10775 (PI: Sarajedini; see Sarajedini et al. 2007). The archive *HST* material is described in Table 1 and consists of images taken through 14 filters spanning a wide spectral range, from the ultraviolet (F225W) to the infrared (F160W). Footprints of *HST* images are shown in Figure 1.

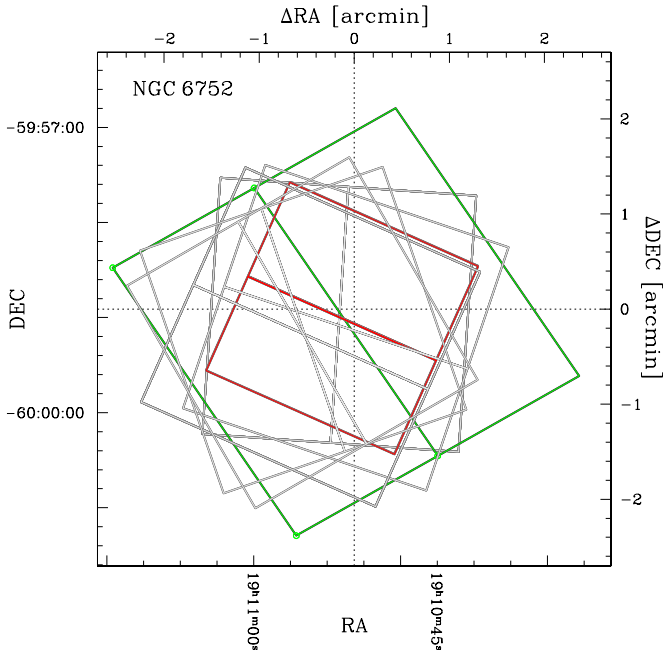

Figure 1. Footprint of the *HST* fields studied in this paper. The footprint of ACS/WFC, WFC3/UVIS, and WFC3/NIR images are colored green, gray, and red, respectively.
(A color version of this figure is available in the online journal.)

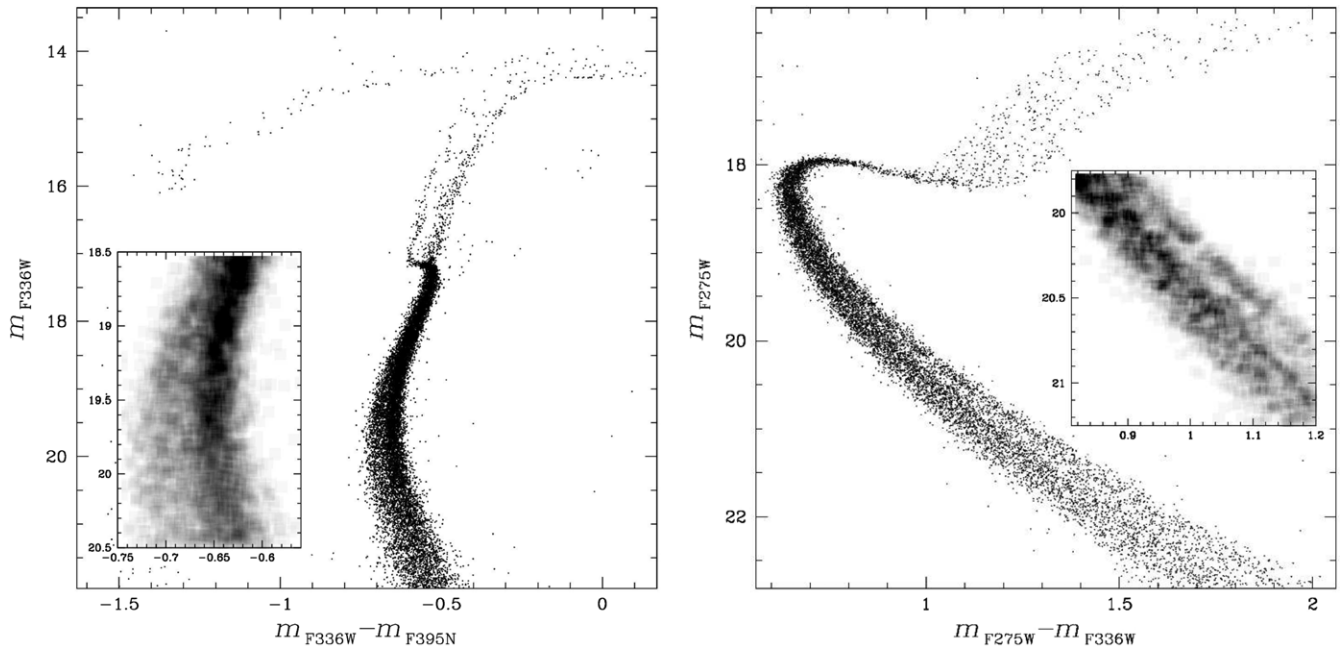

Figure 2. m_{F336W} vs. $m_{F336W} - m_{F395N}$ (left panel) and m_{F275W} vs. $m_{F275W} - m_{F336W}$ CMDs of NGC 6752. The insets show the Hess diagram of a zoomed section of the MS.

The photometry and relative positions of stars in *HST*/WFC3 images were extracted with the software tools described in Bellini et al. (2010), mostly based on the software described in Anderson et al. (2006). The photometry was calibrated onto the Vega-mag system following the procedures given in Bedin et al. (2005), and using encircled energy and zero points given at STScI's web pages. Star positions were corrected for geometric distortion using the solutions given by Bellini & Bedin (2009) and Bellini et al. (2011) for WFC3/UVIS, Anderson & King (2006) for ACS/WFC, and J. Anderson et al. (in preparation) for WFC3/NIR.

To study the external regions of the cluster, we made use of the ground-based photometric catalog published by Grundahl et al. (2002). They have been obtained with the 1.54 m Danish telescope at La Silla (Chile) through the Strömgren filters u, v, b, y, and cover a field of view of $\sim 6 \times 6$ arcmin centered on the cluster. They were reduced following the method outlined in some detail by Stetson (2005).

The stellar catalogs were purged of poorly measured objects using quality indices that our software produces following the procedure that is described in Milone et al. (2009). Finally, the photometry was corrected for zero-point spatial variations following the recipes in Milone et al. (2012c).

3. A TRIPLE MAIN SEQUENCE IN NGC 6752

A visual inspection of the large number of CMDs that we obtain from our data set confirms that multiple sequences along the MS and the RGB can be easily identified by using different combinations of the F275W, F336W, and F395N filters. The left-hand panel of Figure 2 shows the m_{F336W} versus $m_{F336W} - m_{F395N}$ CMD after that the photometric corrections and the quality selection described in the previous section were applied. We note a bimodal RGB and a spread MS. The m_{F275W} versus $m_{F275W} - m_{F336W}$ CMD plotted in the right panel reveals an even larger number of features, with a possible triple RGB, and a clear split MS composed of two distinct components, a narrow red MS, containing about one-fourth of MS stars, and a more dispersed blue MS.

In recent papers, we have shown that two-color diagrams obtained by combining a far-UV filter (such as F225W or F275W), a near-UV filter (such as F336W), and a visible filter (such as F438W) are a powerful way to identify populations of stars with different helium and light-element abundances (see Milone et al. 2012a, 2012b for results on 47 Tuc and NGC 6397).

Motivated by these results, in Figure 3(a) we plot $m_{F275W} - m_{F336W}$ against $m_{F336W} - m_{F410M}$ for MS stars with $19.65 < m_{F275W} < 23.25$. Panel (b) shows the same two-color diagram for the RGB stars.

We also defined the color index $c_{F275W,F336W,F410M} = (m_{F275W} - m_{F336W}) - (m_{F336W} - m_{F410M})$. Quite interestingly, the m_{F275W} versus $c_{F275W,F336W,F410M}$ color-index–magnitude diagram (CMD) of Figure 3(c) allows us to identify multiple sequences along the entire CMD, from the MS to the RGB tip. There is a clear color spread, with the presence of three RGBs and two distinct MSs, in close analogy with what was observed in 47 Tuc and NGC 6397. Also, the SGB is not consistent with a simple stellar population. In the following, we will refer to the less-populated MS located on the bottom left of the two-color diagram in Figure 2(a), as MSa. The MS is analyzed in this section, while Sections 4 and 5 are dedicated to the SGB and the RGB.

In Milone et al. (2010), we used high-precision photometry of ACS/*HST* images to search for signs of multiple populations in NGC 6752. We found a broadened MS and demonstrated that this broadening is intrinsic. We also noted a possible MS bimodality and suggested that the MS split could be due to two stellar populations with almost the same age and iron abundances, but different helium contents. As demonstrated in the following, the data set presented in this paper allows us to identify multiple populations with different helium contents with a higher accuracy than was possible for Milone et al. (2010) with the data available at that time.

Both theoretical arguments and observations indicate that CMDs with wide color baselines can be very sensitive to helium differences among stars (e.g., D'Antona et al. 2005; Piotto et al. 2007). In this context, the m_{F814W} versus $m_{F275W} - m_{F814W}$

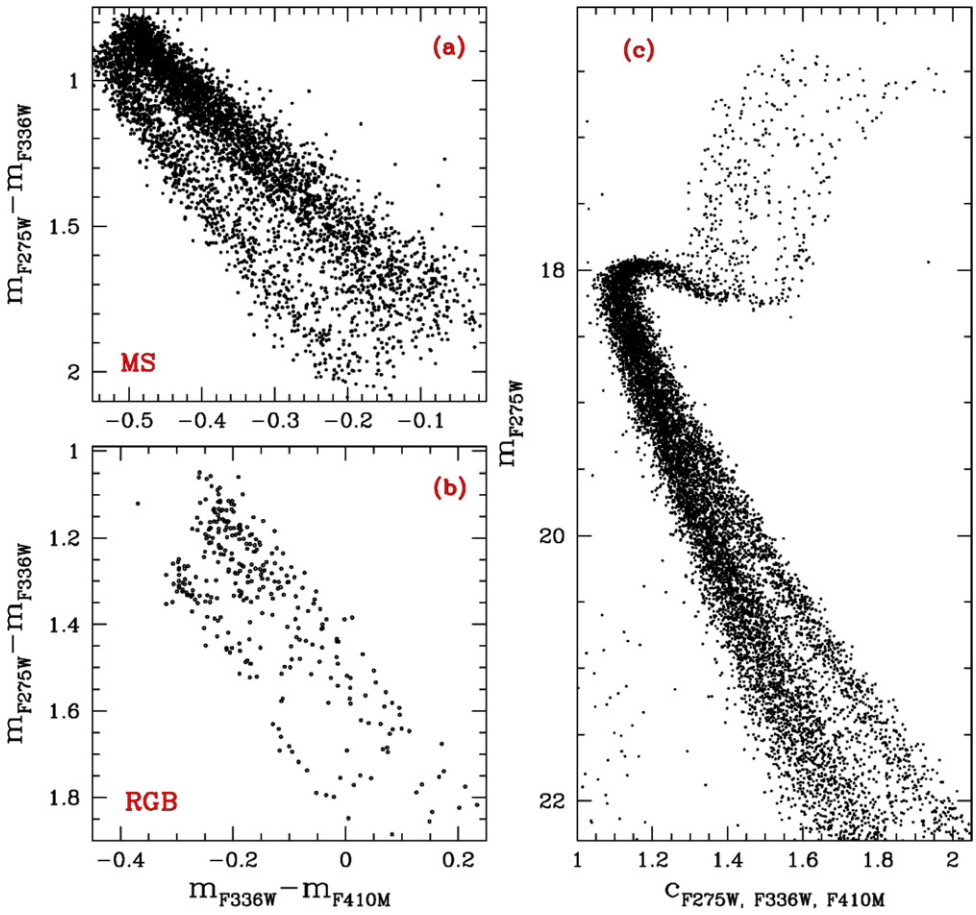

Figure 3. $m_{F275W} - m_{F336W}$ versus $m_{F336W} - m_{F410M}$ two-color diagram for MS stars with $19.65 < m_{F275W} < 23.25$ (panel (a)), and for RGB stars with $m_{F275W} < 18.0$ (panel (b)). Panel (c): the m_{F275W} versus $c_{F275W,F336W,F410M}$ diagram for all NGC 6752 stars in our sample.
(A color version of this figure is available in the online journal.)

CMD shown in Figure 4 clearly reveals a bimodal MS. The MS bimodality is even more evident in the Hess diagram plotted in the inset. The two MSs merge close to the turn-off, and the MS separation increases toward fainter magnitudes, from about 0.1 mag at $m_{F814W} \sim 19.05$ up to 0.25 mag at $m_{F814W} \sim 20.15$. Hereafter, we will refer to the bluest MS of Figure 4 as MSc. We will also demonstrate that the MSa and the MSc correspond to different stellar populations. Note the different morphology (i.e., different distribution in color of the stars) of the MSs plotted in Figures 4 and 2, right panel.

In order to compare the sequences identified in this "regular m_{F814W} versus $m_{F275W} - m_{F814W}$ CMD" with those identified in the m_{F275W} versus $c_{F275W,F336W,F410M}$ CMD of Figure 2(c), we color-code the MSa stars green, and the MSc stars in blue (see panels (a) and (b) of Figure 5). Panel (c) of Figure 5 shows that MSa stars are distinct from MSc, and that MSa + MSc stars are not all MS stars in NGC 6752. In the bottom panels of Figure 5, we identify the MSa and MSc stars in *both* panels and identify as "MSb" stars those that are neither MSa nor MSc. These stars are colored magenta.

This approach allowed us to demonstrate that the MSa and the MSc correspond to two distinct stellar populations, and that NGC 6752 hosts at least a third MS population, labeled as MSb.

The method used to estimate the fraction of stars in the MSa is illustrated in Figure 6. The left-hand panel of the figure is a

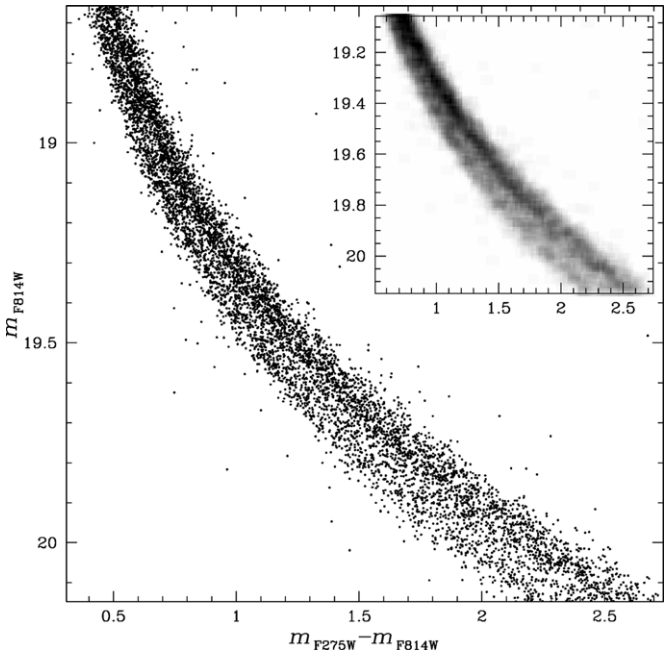

Figure 4. m_{F814W} vs. $m_{F275W} - m_{F814W}$ CMD for MS stars of NGC 6752. The Hess diagram in the inset is a zoom of the region where the MS bimodality is more evident.

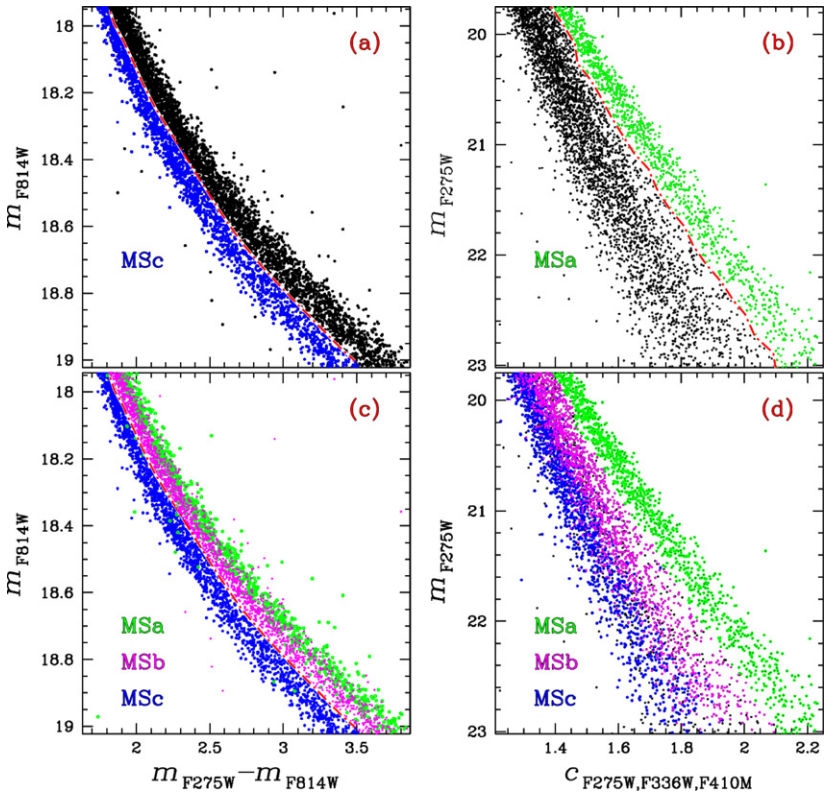

Figure 5. Visualization of the procedure to define the sample of MSa, MSb, and MSc stars. The red dash-dotted lines in panels (a) and (b) are used to select MSc and MSa stars that we colored blue and green, respectively. In panels (c) and (d), we adopted a magenta color to identify stars that belong neither to the MSa nor to the MSc, and hence are part of the third MS component (MSb).

(A color version of this figure is available in the online journal.)

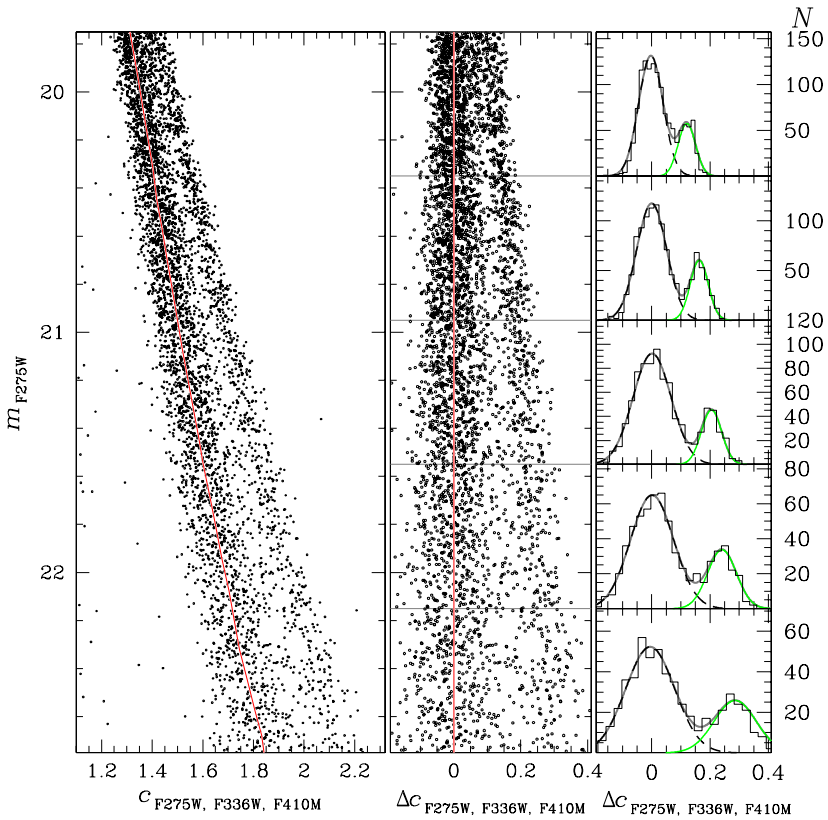

Figure 6. Left panel: reproduction of the diagram of Figure 3(c), where the red line is the fiducial of the most populous MS. Middle panel: the same diagram, after subtraction of the color of the fiducial line. Right panel: the $\Delta c_{F275W,F336W,F410M}$ color distribution in five m_{F275W} intervals. The gray lines represent the least-square best fits of two Gaussians to the observed distribution.

(A color version of this figure is available in the online journal.)

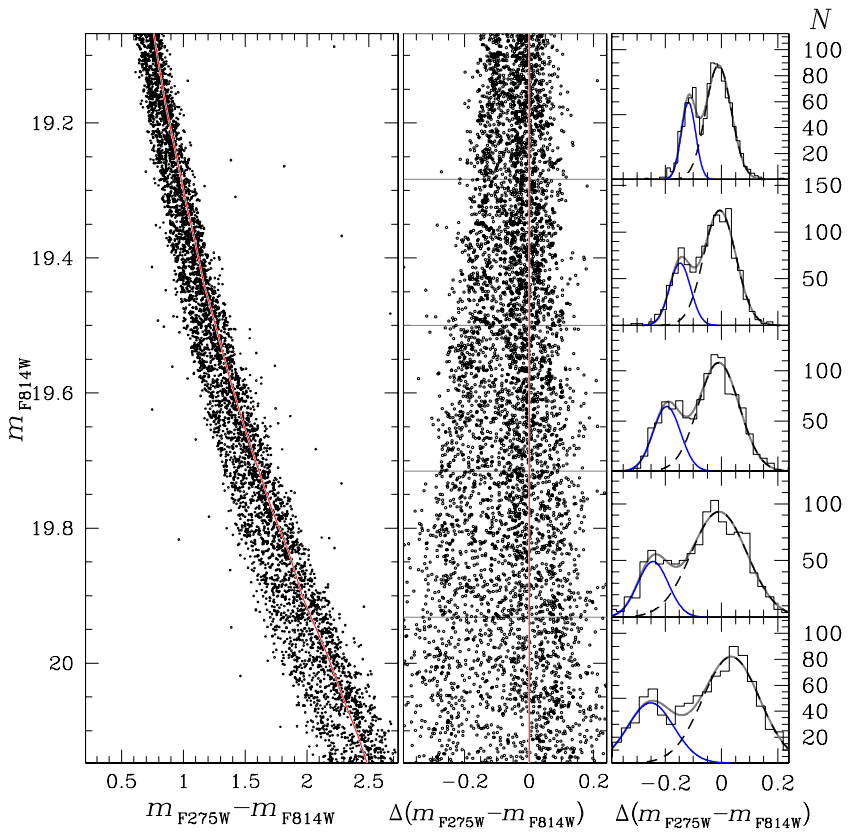

Figure 7. m_{F814W} vs. $m_{F275W} - m_{F814W}$ CMD and verticalized m_{F814W} vs. $\Delta(m_{F275W} - m_{F814W})$ diagram (left and middle panels). The right panels show the histogram of the color distribution in five m_{F814W} intervals. The gray lines represent the least-square best fits of two Gaussians to the observed distribution.

(A color version of this figure is available in the online journal.)

reproduction of the CMD of Figure 3(c) with the fiducial line of the most populated MS superimposed. The verticalized MS is plotted in the middle panel and the right-hand panels show the histograms of the $\Delta(c_{F275W,F336W,F410M})$ color distribution in five m_{F275W} intervals. We fitted each histogram with the sum of two Gaussians, colored green and black. Hereafter, the green color code will be used to highlight MSa stars. From the area under the Gaussians, we estimate that 25% ± 2% of stars belongs to MSa. The errors were computed as the rms of the values obtained for the five bins, and then divided by two (i.e., the square root of the number of bins minus one).

The procedure used to obtain the fiducial line and to verticalize the MS has been adopted in several previous papers from our group (e.g., Piotto et al. 2007), and will be used several times in the remaining part of this paper. Briefly, we adopt the most populous (in this CMD, the bluest) MS as reference sequence and draw by hand a first approximation ridgeline. We also select a color range around this line to include most of the stars on the blue MS. Then, we divide the reference sequence in 0.15 mag intervals and calculate the median colors of the stars within each interval. These median points are then interpolated with a spline. We calculate the spline at the magnitude level of each star and subtracted it from each star's color to estimate the MSRL residual for each. We then determined a sigma-clipped mean for each magnitude interval and repeated the procedure several times. The result is the fiducial line plotted in Figure 6. Finally, we subtract from the $c_{F275W,F336W,F410M}$ color of each star the corresponding color on the fiducial line at the same m_{F275W}.

In order to calculate the fraction of MSc stars, we followed a recipe similar to the one already applied to the MSa, and illustrated in Figure 7. In the left-hand panel, we plotted the m_{F814W} versus $m_{F275W} - m_{F814W}$ CMD, while in the central panel, we show the verticalized CMD, obtained with the same procedure as explained above. The color distribution histograms for five magnitude intervals are shown in the right-hand panels and are fitted with two Gaussians colored blue and black. In the following, the blue color will be used to indicate MSc stars. From the area under the best-fit Gaussians, we estimate that 31% ± 3% of the total number of MS stars belong to MSc. Errors are calculated as described above for the case of the MSa. Since we have already estimated that the MSa and the MSc contain 25% ± 2% and 31% ± 3% of the total number of MS stars, we can conclude that the MSb is made up of the remaining 44% ± 4% of MS stars.

With these identifications and the large number of filters through which we have observations, we can analyze the relative location of the three MSs in a large number of CMDs. As an example, the left panel of Figure 8 shows the m_{F336W} versus $m_{F336W} - m_{F390W}$ CMD for MS stars. In the right panel, we plotted the same CMD, but using the same color codes previously defined in order to highlight MSa, MSb, and MSc stars. Contrary to what is observed in the $m_{F275W} - m_{F814W}$ color in Figure 3 (or in Figure 4), in this CMD, the MSa is bluer than the bulk of MS stars, with the MSb and the MSc being almost coincident.

In order to follow the behavior of the three MSs in all the possible combinations of the photometric bands available in our data set, we followed the approach illustrated in Figure 9. In each panel, we show the fiducial lines of the three MSs in the m_{F814W} versus $m_X - m_{F814W}$ (or $m_{F814W} - m_X$) plane, where X = F225W, F275W, F336W, F390M, F390W, F395N, F410M,

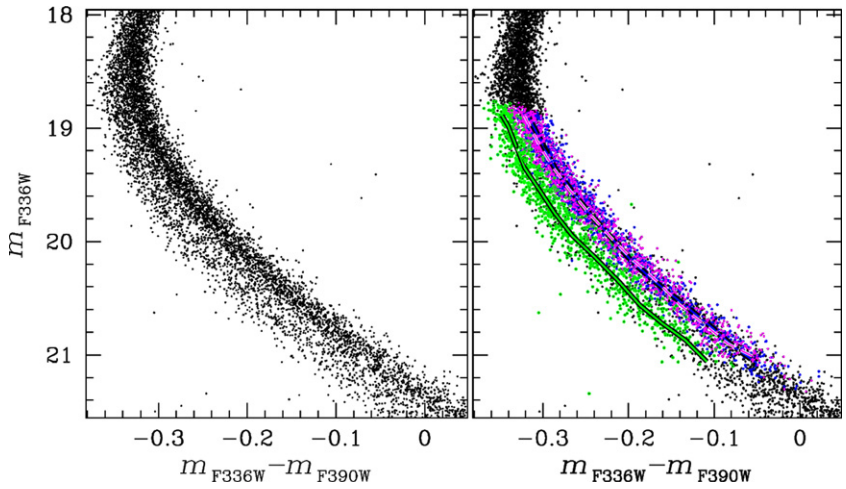

Figure 8. Left panel: m_{F336W} vs. $m_{F336W} - m_{F390W}$ CMD for MS stars. Right panel: an example of the definition of the fiducial lines. The sample of MSa, MSb, and MSc stars defined in Figure 5 are colored green with black shadow, magenta with white shadow, and blue with black shadow, respectively. In this case, the MSb and MSc fiducials are largely overlapping. The same color codes adopted in the previous figures are also used to represent the corresponding fiducials.

(A color version of this figure is available in the online journal.)

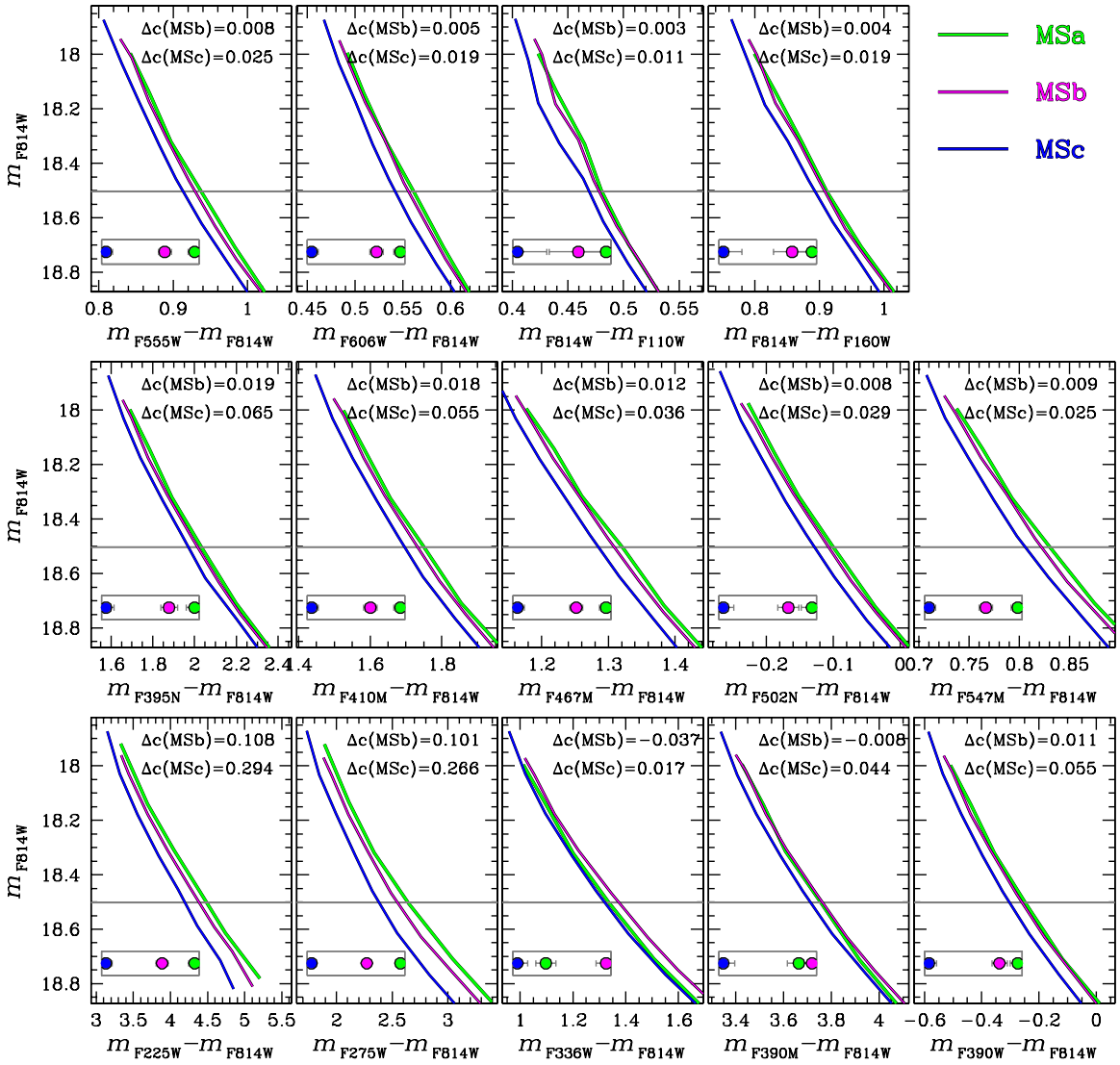

Figure 9. MS fiducials in 14 m_{F814W} vs. $m_X - m_{F814W}$ (or $m_{F814W} - m_X$) CMDs (X = F225W, F275W, F336W, F390M, F390W, F395N, F410M, F467M, F502N, F547M, F555W, F606W, F110W, and F160W). At the top of each panel, we give the color distance from the MSa of the other two MSs, measured at $m^{cut}_{F814W} = 18.5$. The positions of MSa, MSb, and MSc at $m^{cut}_{F814W} = 18.5$ are represented with green, magenta, and blue circles, respectively, in the inset of each CMD.

(A color version of this figure is available in the online journal.)

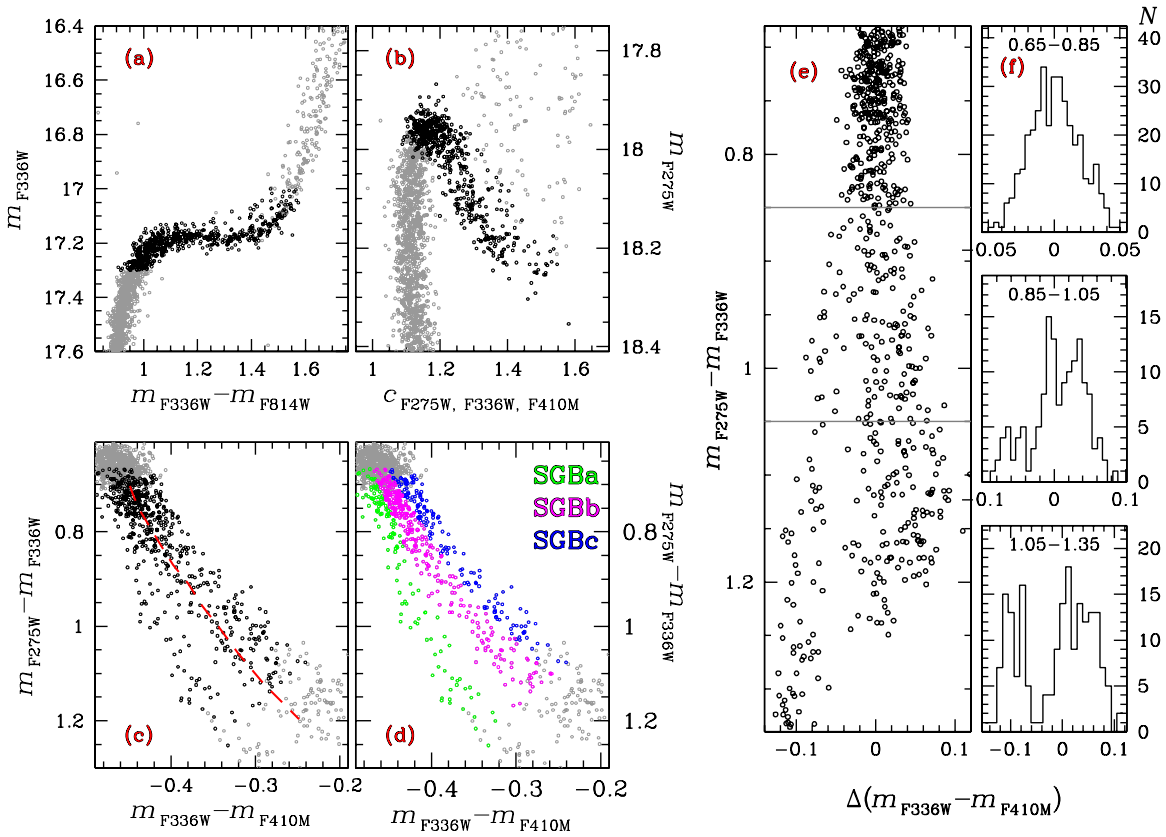

Figure 10. m_{F336W} vs. $m_{F336W} - m_{F814W}$ CMD (panel (a)) and m_{F275W} vs. $c_{F275W,F336W,F410M}$ diagram (panel (b)) zoomed around the SGB. SGB stars are highlighted in thick black. Panel (c): $m_{F275W} - m_{F336W}$ vs. $m_{F336W} - m_{F410M}$ two-color diagrams for the stars shown in the upper panels. The red-dashed line is a fiducial line drawn by hand through the middle SGB. In panel (d), three groups of SGBa, SGBb, and SGBc stars are defined and color-coded in green, magenta, and blue, respectively. The verticalized $m_{F275W} - m_{F336W}$ vs. $\Delta(m_{F336W} - m_{F410M})$ is plotted in panel (e), while the histogram of the distribution in $\Delta(m_{F336W} - m_{F410M})$ is shown in panels (f) for the three quoted $m_{F275W} - m_{F336W}$ intervals.

(A color version of this figure is available in the online journal.)

F467M, F502N, F547M, F555W, F606W, F110W, and F160W. For the two IR filters, F110W and F160W, we adopted the $m_{F814W} - m_X$ color baseline, with X in these cases being the redder filter.

The MSs color properties in the various CMDs can be summarized as follows:

1. The MSb is typically bluer than the MSa in all CMDs of Figure 9, with the exception of the m_{F814W} versus $m_{F336W} - m_{F814W}$ and the m_{F814W} versus $m_{F390M} - m_{F814W}$ CMDs, where the two sequences invert their relative colors.
2. The MSc is bluer than the MSa in all CMDs.
3. The color distance between the MSa and both the MSb and the MSc increases for larger color baselines, with the exception of the $m_{F336W} - m_{F814W}$, the $m_{F390M} - m_{F814W}$, and the $m_{F390W} - m_{F814W}$ colors.
4. The color separation between the MSc and the MSb increases with the size of the color baseline for all colors studied in this paper.

In the following, we will use these data to gather information on the chemical composition of the three MSs.

4. MULTIPLE STELLAR POPULATIONS ALONG THE SUBGIANT BRANCH

The first photometric evidence of multiple stellar populations along the SGB of NGC 6752 comes from the recent paper by Kravtsov et al. (2011). Using wide-field ground-based photometry, Kravtsov et al. (2011) identified a spread of ∼0.3 mag in the U band, with the faintest SGB more centrally concentrated than its brighter counterpart.

Our multi-color set of CMDs reveals an even more complex picture for the SGB of NGC 6752. A visual inspection at the m_{F336W} versus $m_{F336W} - m_{F814W}$ CMD and the m_{F275W} versus $c_{F275W,F336W,F410M}$ diagram in the upper panel of Figure 10 immediately reveals that in the WFC3/UVIS field of view, there is *no* evidence for a wide magnitude spread along the SGB in F336W (which is the *HST* analog of the standard U), even though the SGB is clearly not consistent with a single stellar population. By analogy with what we did for the MS stars, in the lower panels of Figure 10, we plot the $m_{F275W} - m_{F336W}$ versus $m_{F336W} - m_{F410M}$ two-color diagram. This diagram shows a multimodal distribution of SGB stars (see also the histograms of panels (f)). As shown in the figure, we selected by eye three groups of SGB stars that we named SGBa, SGBb, and SGBc and colored them green, magenta, and blue, respectively.

In order to better understand the properties of these three sequences, Figure 11 gives a 4 × 4 array of CMDs, where stars of the three sequences selected in Figure 10 are plotted with their color code. Figure 11 shows some significant features of the SGB of NGC 6752:

1. SGBa stars share some similarities with MSa: they are on average redder than the bulk of SGB stars in $m_{F275W} - m_{F336W}$, but they become bluer than the remaining SGB stars in the other CMDs of the first row of Figure 11.
2. In the F336W band, SGBa stars are typically brighter than the other SGB stars. This fact also explains why they appear

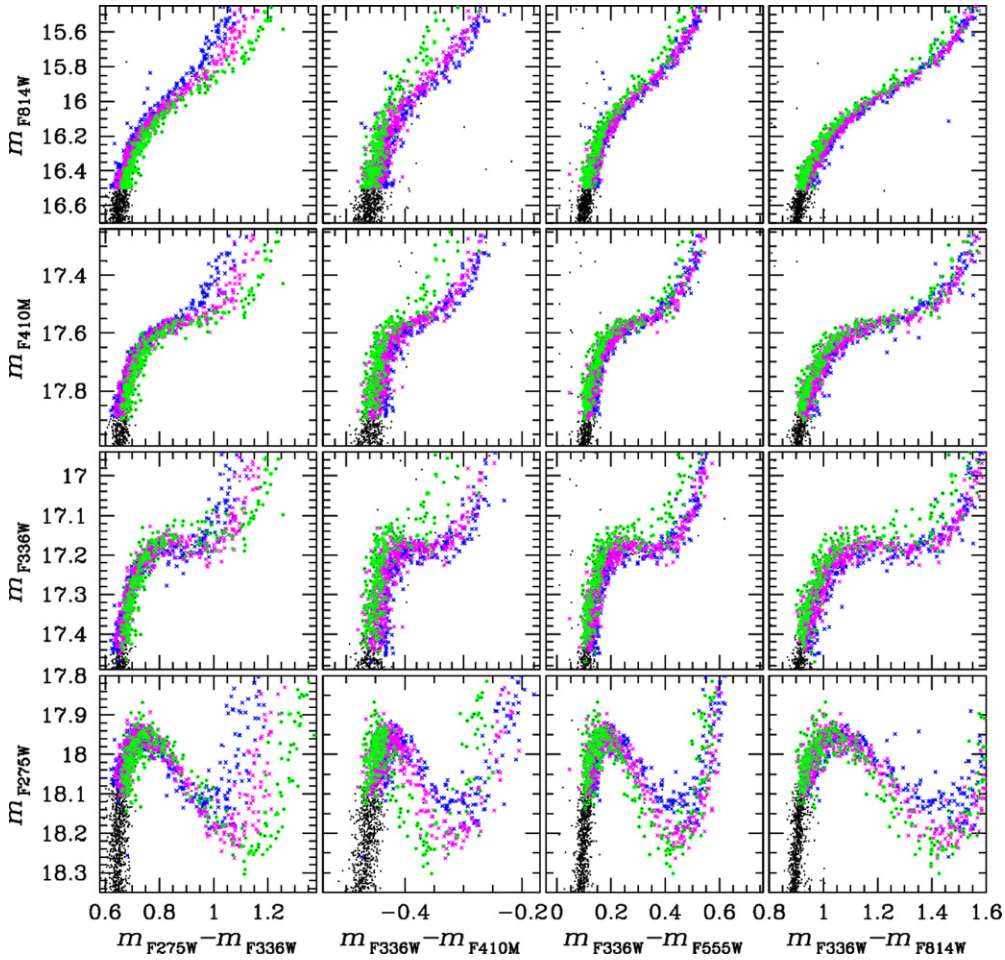

Figure 11. Collection of CMDs zoomed around the SGB. SGBa, SGBb, and SGBc stars defined in Figure 10(d) are plotted green, magenta, and blue, respectively.
(A color version of this figure is available in the online journal.)

redder than SGBb and SGBc stars in $m_{F275W} - m_{F336W}$, and bluer than them in the other CMDs of the third row of Figure 11.

3. In all the CMDs, the SGBb sequence seems to be located between the SGBa and the SGBc.

The analogy in color distribution of the three MSs and SGBs justifies the names that we gave to these sequences, which explicitly want to suggest that the SGBa, SGBb, and SGBc represent the continuation along the CMD of the MSa, MSb, and MSc, respectively.

5. MULTIPLE STELLAR POPULATIONS ALONG THE RED-GIANT BRANCH

As already mentioned in Section 1, the first evidence that the RGB of NGC 6752 is not consistent with a single stellar population comes from Grundahl et al. (2002), *followed by* Yong et al. (2008), Milone et al. (2010), Kravtsov et al. (2011), and Carretta et al. (2012). These studies have detected a large spread in the c_y Strömgren index[11] with the presence of three RGBs. The large data set listed in Table 1 allowed us to add further information on the multimodal RGB of NGC 6752.

To extend our multi-wavelength study of the RGB, we attempted to identify the sequences corresponding to each stellar population along the RGB. We already noted that the m_{F275W} versus $c_{F275W,F336W,F410M}$ diagram of Figure 3 shows a triple RGB. In Figure 12 (panel (a)), we isolated by hand three groups of stars. Hereafter, we will name these three groups RGBa, RGBb, and RGBc, colored green, magenta, and blue, respectively. The red fiducial line is obtained with a procedure similar to the one introduced in Section 3 for MS stars. The only difference is that for RGB stars, we used a second-order polynomial to interpolate the median color and magnitude values measured in the different magnitude intervals.

The verticalized m_{F275W} versus $\Delta c_{F275W,F336W,F410M}$ diagram is plotted in panel (b) of Figure 12, while panel (c) of the same figure shows the histogram of the distribution in $\Delta c_{F275W,F336W,F410M}$. The histogram is fitted by the sum of three Gaussians which we colored green, magenta, and blue, respectively. From the area of the Gaussians, we derive the relative fraction of RGBa, RGBb, and RGBc stars to be (0.31 ± 0.03, 0.41 ± 0.02, 0.28 ± 0.03).

In order to get additional information on the three RGBs from all possible combinations of magnitudes in the photometric passbands of our data set, we follow the same procedure for the RGB stars that we performed in Section 3 for the MS. The results are illustrated in Figure 13 where we show the fiducial polynomials in 12 m_{F814W} versus $m_X - m_{F814W}$ CMDs, where $X =$ F225W, F275W, F336W, F390M, F390W, F395N, F410M, F467M, F502N, F547M, F555W, and F606W. In this analysis, we did not include the F110W and F160W filters because the

[11] The index c_y is defined as $c_y = c_1 - (b - y)$, where $c_1 = (b - v) - (v - b)$ (Yong et al. 2008).

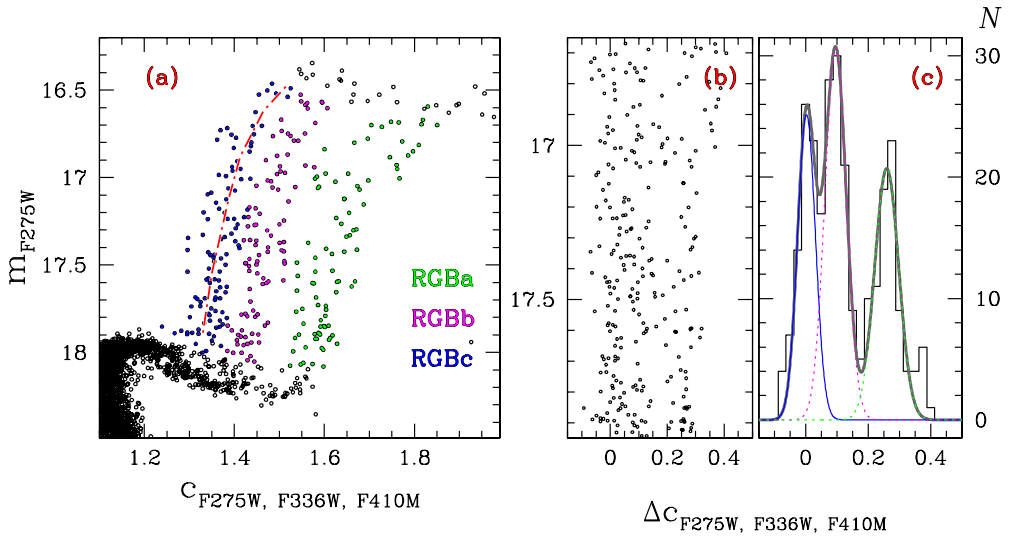

Figure 12. Panel (a): zoom in of the m_{F275W} vs. $c_{F275W,F336W,F410M}$ diagram of Figure 3(c) around the RGB. Selected RGBa, RGBb, and RGBc stars are plotted green, magenta, and blue, respectively. Panel (b): verticalized diagram for RGB stars with $16.65 < m_{F275W} < 17.95$. Panel (c): histogram of the distribution of stars shown in panel (b). The gray line is the best-fitting least-square function defined as the sum of the green, magenta, and blue Gaussians.

(A color version of this figure is available in the online journal.)

RGB fiducials are poorly determined in these colors on account of the small number of RGB stars that have IR photometry. This is a consequence of three main facts: (1) the IR/WFC3 camera has a smaller field of view than UVIS/WFC3, (2) due to its large pixel scale, the IR/WFC3 detector is more affected by crowding, hence the fraction of stars with high-accuracy photometry is smaller, and (3) IR photometry saturates a couple of magnitudes above the MS turn-off.

Both RGBb and RGBc are typically bluer than RGBa, with the exception of CMDs based on the $m_{F336W} - m_{F814W}$ and $m_{F390W} - m_{F814W}$ colors. In the other filters, the color distance from RGBa of both RGBb and RGBc increases with the color baseline, with the possible exception of $m_{F390M} - m_{F814W}$ and $m_{F395N} - m_{F814W}$. A comparison of Figures 9 and 13 reveals that the behavior of the three RGBs and the three MSs is quite similar, and it will be discussed in Section 6.

5.1. The Chemical Composition of the Three Stellar Populations

In the past three decades, many spectroscopic studies have provided us with an accurate picture of the chemical composition of NGC 6752 (e.g., Norris et al. 1981; Grundahl et al. 2002; Yong et al. 2003, 2005, 2008; Carretta et al. 2007, 2012). We know that NGC 6752 is a moderately metal poor ([Fe/H] ~ -1.6; Yong et al. 2005; Carretta et al. 2010) GC, with large star-to-star variations in O, N, Na, Mg, and Al. Nitrogen is correlated with aluminum and sodium, and has a possible small amplitude correlation with α, Fe-peak, and *s*-process elements (Yong et al. 2008). Both the Na–O and Mg–Al anticorrelations have been observed by Yong et al. (2005) and Carretta et al. (2007, 2009, 2012).

Strömgren photometry can provide additional, important information on the chemical properties of the stellar populations. Grundahl et al. (2002) and Sbordone et al. (2011) have demonstrated that the c_y index correlates with the nitrogen abundance, and hence can be used to identify different stellar populations in GCs. Other combinations of Strömgren filters are sensitive to the chemical differences of GC stars (see, e.g., Grundahl et al. 2000; Marino et al. 2011; Carretta et al. 2011).

The y versus $(u-b)-(v-y)$ diagram of NGC 6752 is shown in Figure 14, in the upper panel (see Carretta et al. 2011 for a discussion on this color index). To avoid the central cluster regions where the photometric error is larger because of crowding, in the upper panel of Figure 14, we show stars with a distance from the center larger than 1.7 arcmin. As already pointed out by Grundahl et al. (2002), in Strömgren photometry CMDs, the RGB shows three main components. We investigated whether these three RGBs correspond to the three populations we have identified in this paper. To do this, we cross-identified the stars in the *HST* and Strömgren catalog and in the CMD in the inset of the upper panel of Figure 14 (which includes only stars out to 1.7 arcmin from the cluster center), and we colored green, magenta, and blue the RGBa, RGBb, and RGBc stars identified in Figure 12. Even if the stars common to both the *HST* and Strömgren data sets are all located near the cluster center—and hence have larger photometric errors—it is clear that stars in RGBa, RGBb, and RGBc have a different location (color) in the CMD from Strömgren photometry.

In order to estimate the number of stars in each RGB, we first isolated the RGB region with $13.5 < y < 16.5$ and distance from the center larger than 1.7 arcmin, and drew by hand a fiducial line through the middle RGB as illustrated in the bottom-left panel of Figure 14. Then, we verticalized the RGB following the procedure described in Section 3 (middle lower panel of Figure 14). Finally, we obtained the histogram of the $\Delta((u-b)-(v-y))$ color distribution shown in the right panels of Figure 14. The histogram was least-squared fitted with three Gaussians. By summing the area under the three Gaussians, we find that the fractions of RGBa, RGBb, and RGBc stars at radial distances between 1.7 and 6.1 arcmin are 27% ± 4%, 44% ± 4%, and 29% ± 3%, respectively. The quoted uncertainties are Poisson errors and represent a lower limit of the true errors. All methods applied thus far to the MS and RGB yield very similar fractions of the a, b, and c populations, suggesting an association between the MS and RGB for the three populations.

Available spectroscopic abundances allow us to better characterize the chemical content of each single RGB. Figure 15 reproduces the correlations among Al, Mg, N, Na, and O using the chemical abundance measurements by Yong et al. (2005,

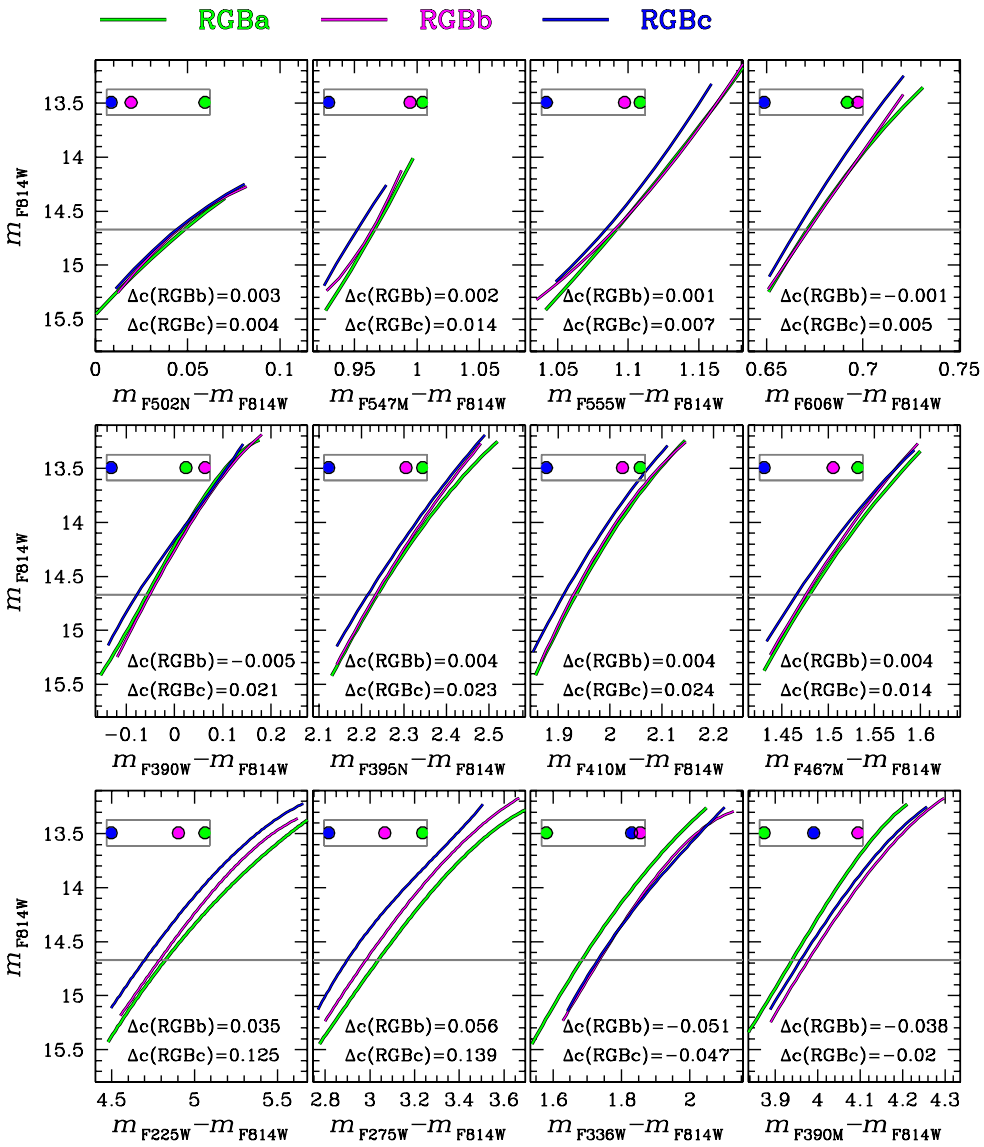

Figure 13. RGB fiducials in 12 m_{F814W} vs. $m_X - m_{F814W}$ CMDs (X = F225W, F275W, F336W, F390M, F390W, F395N, F410M, F467M, F502N, F547M, F555W, and F606W). The color distance from the RGBa, measured at $m^{cut}_{F814W} = 14.7$, is indicated in each panel. The positions of RGBa, RGBb, and RGBc at $m^{cut}_{F814W} = 14.7$ are represented with green, magenta, and blue circles, respectively, in the inset of each CMD.

(A color version of this figure is available in the online journal.)

2008). In the upper-right panel, we arbitrarily selected three groups of Na-poor, Na-intermediate, and Na-rich stars and colored them green, magenta, and blue, respectively. These color codes are used consistently in the other panels of this figure.

As Yong and collaborators have already pointed out, Na-rich stars are enhanced in Al, N, and *s*-process elements, and depleted in O and Mg. Na-intermediate stars are also Al, N-enhanced and O-depleted, but their abundance variations are smaller, on average, than those of Na-rich stars. There is no significant difference in the Mg and Y content of Na-poor and Na-intermediate stars. It is interesting to note that the three groups of stars are not chemically homogeneous, as they show star-to-star variation in the abundance of some elements that are significantly larger than observational errors (see Yong et al. 2008 for more details).

In the y versus $(u-v)-(b-y)$ diagram of the left-bottom panel of Figure 15, we mark with full dots the Na-poor, Na-intermediate, and Na-rich stars selected in the upper-leftmost panel. The three RGBs correspond to groups of stars with different light-element content, as first noticed by Grundahl et al. (2002). We have *HST* photometry for only one of the stars observed by Yong et al. (2008). Its position in the m_{F275W} versus $c_{F275W,F336W,F410M}$ diagram is shown in the lower-middle panel and confirms that the RGBc is made of Na-rich stars.

The average abundance for 22 elements from Yong et al. (2008) for the three groups of RGB stars defined above are listed in Table 2. We emphasize how the available spectroscopic measures offer us a precious opportunity to characterize the chemical composition of the stars of the three stellar populations in NGC 6752.

5.2. Some Considerations on the Spectroscopic and Photometric Observational Evidence of Multiple Stellar Populations

The Na–O anticorrelation has been proposed as a possible proof of the presence of multiple stellar generations in star clusters. Several authors suggested that the different populations of stars in GCs can be identified on the basis of their position

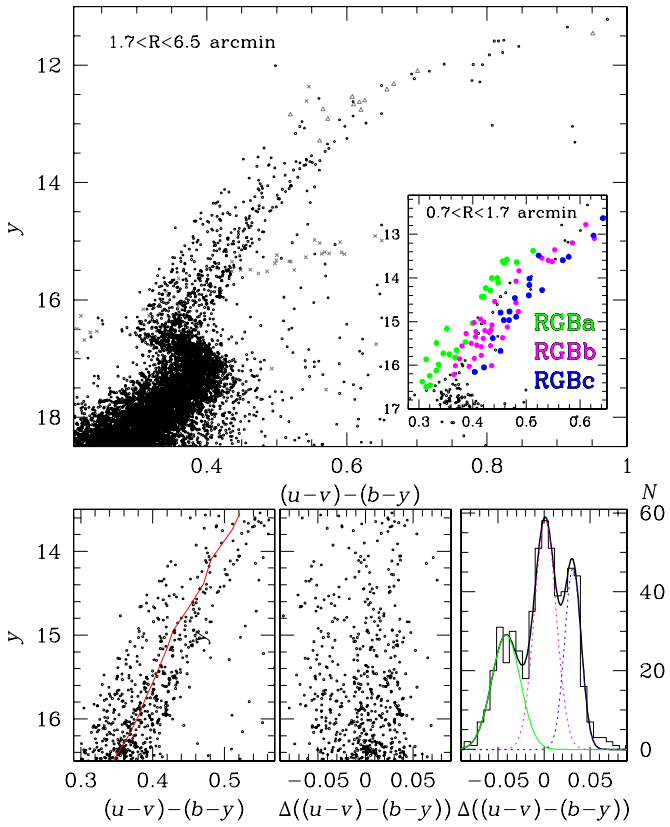

Figure 14. Upper panel: y vs. $(u-v)-(b-y)$ diagram for NGC 6752 obtained using the Strömgren photometric catalog from Grundahl et al. (2002). Only stars with distance from the cluster center greater than 1.7 arcmin are plotted in this panel. Asymptotic giant branch and HB stars, identified in the b vs. $v-y$ CMD are represented with gray triangles and crosses, respectively. The inset is a zoom around the RGB for stars with distance from the center $0.7 < R < 1.7$ arcmin, where we colored green, magenta, and blue the RGBa, RGBb, and RGBc stars selected in Figure 12. The lower panels illustrate the procedure to estimate the fraction of stars in each RGB. The left panel shows the fiducial line superimposed to the RGBb, the rectified CMD for RGB stars is plotted in the middle panel while right panel shows the histogram of the $\Delta((u-b)-(v-y))$ distribution with the best-fit Gaussian colored green, magenta, and blue.

(A color version of this figure is available in the online journal.)

along the Na–O abundance plane, with the first generation including stars with oxygen and sodium abundances similar to halo field stars at the same metallicity, with the remaining Na-rich/O-poor to be considered as part of a second generation (e.g., Kraft 1994).

Spectroscopic studies show that the Na–O anticorrelation is a common property among GCs (e.g., Ramírez & Cohen 2002; Carretta et al. 2009, 2010 and references therein). However, there clearly is a problem we have not solved yet. Figure 12 from the compilation by Ramírez & Cohen (2002) and Figure 1 by Carretta et al. (2010) show an almost continuous distribution of stars in the Na versus O plane, despite the fact that photometric evidence in many of the clusters included in that figure (e.g., NGC 2808, NGC 6397, NGC 6752 as shown in the present paper) shows multimodal, possibly discrete, sequences in the CMD when high-accuracy photometry on images collected with the appropriate filters is used.[12] Why do we have this possible difference between the spectroscopic and the photometric manifestation of the multiple stellar populations in GCs?

[12] Note however that, in some cases, multimodal distribution in Na and O has been detected also from high-resolution spectroscopic (see e.g., Yong et al. 2008; Marino et al. 2008; Lind et al. 2011 for the cases of NGC 6752, M 4, and NGC 6397).

Carretta et al. (2009) suggested criterion to separate stellar populations on the basis of their position in the Na–O plane. They defined as the primordial (P) component all stars with an [Na/Fe] ratio in the range between $[Na/Fe]_{min}$ and $[Na/Fe]_{min} + 0.3$, where $[Na/Fe]_{min}$ is the minimum value of the ratio [Na/Fe] ratio estimated by eye. The remaining stars are considered all second-population stars, and have been further divided into two groups. Stars with ratio $[O/Na] > -0.9$ dex belong to the intermediate (I) population, while those with $[O/Na] < -0.9$ dex are defined as the extreme (E) population. Clearly, this separation is arbitrary and not based on any feature (gaps or peak) in the NaO diagram, *and it has* no clear physical meaning. As an example, in Figure 16, we apply the same criteria as proposed by Carretta et al. (2009) to the sample of NGC 6752 stars studied by Yong at al. (2008) and further analyzed in Section 5.1. The two red segments define the regions in the Na–O plane populated by P, I, and E stars, and are determined following the recipes by Carretta and collaborators. The stars of the Populations a, b, and c identified in this paper are colored green, magenta, and blue, respectively. Figure 16 shows that (1) the Carretta et al. (2009) P component includes all the stars in Population a but is contaminated by Population b stars, (2) the I component contains both Population b and Population c stars, and (3) no stars belong to the E component. Apparently, the general criteria introduced by Carretta et al. (2009) do not apply to NGC 6752.

The main problem here is not related to the meaning of the Carretta et al. (2009) definition. The problem is that there still is an inconsistency between what we observe with spectroscopy (a continuous distribution along the Na versus O plane) and what accurate, high-precision photometry tells us, i.e., that most clusters host distinct, separate evolutionary branches in the CMD. It is important to understand whether this is just the consequence of the (internal) errors in the measurement of Na and O abundances, or whether there is some underlying physical reason we have not yet understood.

6. THE HELIUM ABUNDANCE OF THE THREE STELLAR POPULATIONS OF NGC 6752

In this section, we will use the multicolor *HST* photometry to further characterize the chemistry of the different stellar populations in NGC 6752 and estimate the helium abundances of its three stellar populations. The multi-dimensional space of our CMDs makes it difficult to visualize fitting isochrones to our sequences. To make the comparison easier, we will quantify the color separation between the sequences at two fiducial points at the level of the MS and the RGB.

In all 14 CMDs of Figure 9, we calculated the color differences between MSa, MSb, and MSc at the reference magnitude $m^{cut}_{F814W} = 18.5$. These color differences are calculated by subtracting from the color of the MSa fiducial at $m^{cut}_{F814W} = 18.5$ the color of the MSb (or MSc) fiducial at the same luminosity. The left panel of Figure 17 shows the measured color difference as a function of the central wavelength of the m_X filter.

It is now clear why the $c_{F275W,F336W,F410M}$ index is an efficient tool to identify multiple sequences in the CMD. Indeed, Figure 17 shows that both the $m_{F275W} - m_{F336W}$ and the $m_{F336W} - m_{F410M}$ color provide large separations between the MSa (or the RGBa) and the other two MSs (RGBs). The MSa (RGBa) is redder than the MSb and the MSc (RGBb and RGBc) in $m_{F275W} - m_{F336W}$, but it moves to the blue in $m_{F336W} - m_{F410M}$. Therefore, the color index $c_{F275W,F336W,F410M} = (m_{F275W} -$

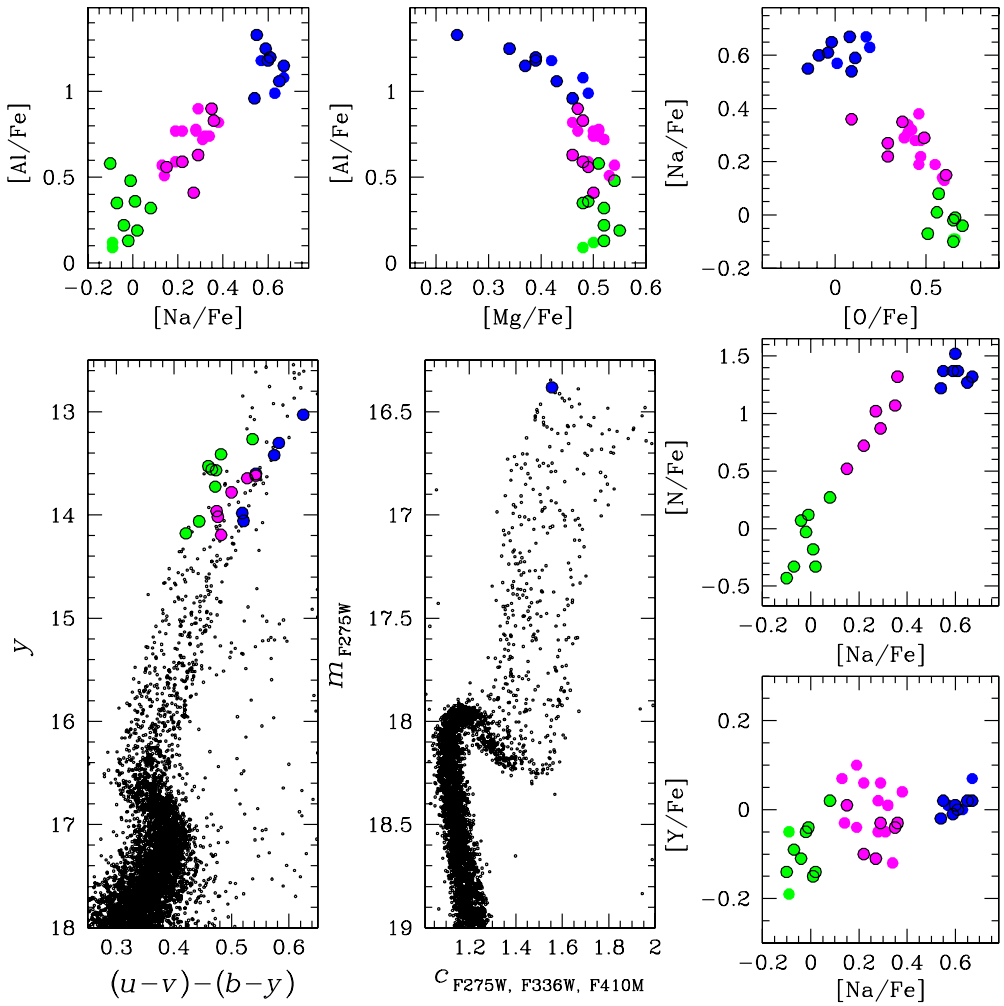

Figure 15. Upper and right panels: correlations and anticorrelations among the abundances of several chemical species from Yong et al. (2003, 2008). We have selected three groups of stars with different [Na/Fe] and colored them green, magenta, and blue. In the bottom-left and central panel, we mark the position of these stars in the v vs. $(u-v)-(b-y)$ diagram and the $m_{\rm F275W}$ vs. $c_{\rm F275W,F336W,F410M}$ diagram. Stars for which both spectroscopic and photometric measurements are available are marked with black circles.

(A color version of this figure is available in the online journal.)

$m_{\rm F336W}) - (m_{\rm F336W} - m_{\rm F410M})$ maximizes the separation among the sequences.[13]

In order to compare these observations with expectations from synthetic photometry, we followed a procedure that has already been used in previous publications (Milone et al. 2012a, 2012b; Bellini et al. 2012, see also Sbordone et al. 2011). Briefly, we used the BaSTI isochrones (Pietrinferni et al. 2004, 2009) for the populations listed in Table 3, and determined $T_{\rm eff}$ and $\log g$ for an MS star with $m^{\rm cut}_{\rm F814W} = 18.5$. To do this, we assumed $E(B-V) = 0.03$ and $(m-M)_{\rm V} = 13.19$ in agreement with the values of reddening and distance modulus listed in Harris (1996; updated as in 2010 December). For the ACS/WFC filters, we used the extinction coefficients tabulated by Bedin et al. (2005) for a cold ($T = 4000$ K) star. For the WFC3/UVIS filters, we linearly interpolated the coefficients tabulated by Bedin et al. (2005), and for WFC3/IR we adopted the values listed in the York Extinction Solver Web site.[14] For each of the three populations, we adopted the abundances of the 22 elements listed in Table 2, which represent the average abundance of the three stellar populations. Since carbon abundance was not measured by Yong et al. (2008) we adopted the [C/Fe] values from Carretta et al. (2005) and take [C/Fe] = 0.15 for Population a, and [C/Fe] = −0.15 for both Populations b and c.

We assumed that the Population a has primordial helium content ($Y = 0.246$), and adopted for both the Populations b and c different helium abundances as described in the following. We used the ATLAS12 code (Kurucz 2005; Castelli 2005; Sbordone et al. 2007) to calculate model atmospheres by using the specific chemical composition of each stellar population, and assuming the temperatures and gravities listed in Table 3. Then, we used the SYNTHE code (Sbordone et al. 2007) to synthesize the spectrum from 1000 Å to 20,000 Å, and the resulting spectra were convolved with the transmission curves of the system formed by the telescope, the camera, and each of our filters to produce the synthetic magnitudes and colors for each photometric band.

The adopted chemical compositions for the three different stellar Populations a, b, and c identified within NGC 6752 (MSs, SGBs, and RGBs) are tabulated in Table 3 for three different options. In all three options, Population a is assumed to have

[13] By following a similar approach, we suggest that other color indices $c_{\rm F336W,F410M,F814W} = (m_{\rm F336W} - m_{\rm F410M}) - (m_{\rm F410M} - m_{\rm F814W})$ can be powerful tools to detect multiple stellar populations in the CMD of GCs. The later is less efficient than $c_{\rm F275W,F336W,F410M}$, but it uses a wavelength range that is accessible to ground-based telescopes.

[14] http://www3.cadc-ccda.hia-iha.nrc-cnr.gc.ca/community

Table 2
Average Chemical Abundance for the Three RGB Components

Population	Population a			Population b			Population c		
Element	Abundance (dex)	σ	N	Abundance (dex)	σ	N	Abundance (dex)	σ	N
[O/Fe]	0.65 ± 0.04	0.11	10	0.43 ± 0.03	0.13	18	0.03 ± 0.04	0.11	10
[N/Fe]	-0.11 ± 0.09	0.25	8	0.92 ± 0.13	0.28	6	1.35 ± 0.04	0.10	7
[Na/Fe]	-0.03 ± 0.02	0.06	10	0.26 ± 0.02	0.08	18	0.61 ± 0.02	0.05	10
[Mg/Fe]	0.51 ± 0.01	0.02	10	0.49 ± 0.01	0.02	18	0.40 ± 0.02	0.07	10
[Al/Fe]	0.28 ± 0.05	0.16	10	0.70 ± 0.03	0.14	18	1.14 ± 0.04	0.12	10
[Si/Fe]	0.27 ± 0.02	0.07	10	0.33 ± 0.01	0.05	18	0.35 ± 0.01	0.04	10
[Ca/Fe]	0.21 ± 0.03	0.08	10	0.24 ± 0.02	0.09	18	0.27 ± 0.02	0.06	10
[Sc/Fe]	-0.05 ± 0.01	0.04	10	-0.04 ± 0.01	0.04	18	-0.04 ± 0.01	0.04	10
[Ti/Fe]	0.10 ± 0.02	0.06	10	0.14 ± 0.01	0.04	18	0.15 ± 0.01	0.03	10
[V/Fe]	-0.34 ± 0.05	0.16	10	-0.29 ± 0.03	0.12	18	-0.25 ± 0.03	0.08	10
[Mn/Fe]	-0.50 ± 0.04	0.11	10	-0.44 ± 0.01	0.06	18	-0.45 ± 0.01	0.04	10
[Fe/H]	-1.65 ± 0.02	0.07	10	-1.61 ± 0.01	0.02	18	-1.61 ± 0.01	0.01	10
[Co/Fe]	-0.03 ± 0.03	0.09	10	-0.00 ± 0.02	0.06	18	-0.06 ± 0.02	0.07	10
[Ni/Fe]	-0.06 ± 0.02	0.07	10	-0.06 ± 0.01	0.04	18	-0.03 ± 0.01	0.03	10
[Cu/Fe]	-0.66 ± 0.03	0.09	10	-0.59 ± 0.01	0.05	18	-0.60 ± 0.01	0.04	10
[Y/Fe]	-0.09 ± 0.02	0.06	10	-0.01 ± 0.02	0.06	18	0.01 ± 0.01	0.02	10
[Zr/Fe]	0.07 ± 0.05	0.15	10	0.20 ± 0.02	0.07	18	0.21 ± 0.03	0.09	10
[Ba/Fe]	-0.09 ± 0.04	0.13	10	-0.12 ± 0.03	0.13	16	0.05 ± 0.02	0.07	9
[La/Fe]	0.12 ± 0.02	0.02	2	0.10 ± 0.01	0.04	12	0.13 ± 0.04	0.06	3
[Ce/Fe]	0.28 ± 0.03	0.09	10	0.25 ± 0.01	0.04	18	0.28 ± 0.02	0.06	10
[Nd/Fe]	0.23 ± 0.01	0.04	10	0.22 ± 0.01	0.05	18	0.23 ± 0.01	0.04	10
[Eu/Fe]	0.31 ± 0.03	0.10	10	0.30 ± 0.02	0.08	18	0.34 ± 0.03	0.10	10

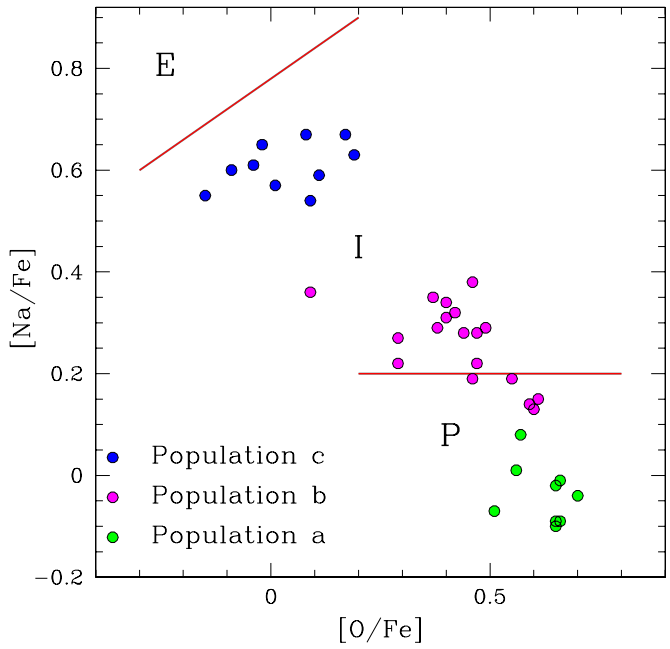

Figure 16. Reproduction of the Na–O anticorrelation from Yong et al. (2008). Stars belonging to the Populations a, b, and c defined in this paper are colored green, magenta, and blue, respectively. The red segments indicate the separation for the P, I, and E components suggested by Carretta et al. (2009).

(A color version of this figure is available in the online journal.)

a canonical helium abundance and the chemical composition in Table 2. Instead, the chemical compositions and the helium fraction (Y) of Populations b and c are different for different options. In detail:

1. In Option I, the three populations have the same chemical composition, but three different values for the helium content ($Y = 0.246$, 0.254, and 0.275).

Table 3
Parameters used to Simulate Synthetic Spectra of an MSa, MSb, and an MSc Star with $m_{F814W} = 18.5$, and an RGB Star with $m_{F814W} = 14.7$ for the Three Assumed Options

MS (Option)	T_{eff}	log g	Y	Chemical Composition (see Table 2)
MSa (all)	5445	4.68	0.246	as for population a
MSb (I)	5470	4.68	0.254	as for population a
MSb (II)	5445	4.68	0.246	as for population b
MSb (III)	5470	4.68	0.254	as for population b
MSc (I)	5534	4.69	0.275	as for population a
MSc (II)	5445	4.68	0.246	as for population c
MSc (III)	5534	4.69	0.275	as for population c
RGBa (all)	5343	3.26	0.246	as for population a
RGBb (I)	5351	3.26	0.254	as for population a
RGBb (II)	5343	3.26	0.246	as for population b
RGBb (III)	5351	3.26	0.254	as for population b
RGBc (I)	5373	3.25	0.275	as for population a
RGBc (II)	5343	3.26	0.246	as for population c
RGBc (III)	5373	3.25	0.275	as for population c

Notes. For all the populations, we assumed [Fe/H] = −1.6. The adopted chemical composition is given in Table 2.

2. In Option II, the three populations have the same helium fraction, but the three chemical compositions given in Table 2.
3. In Option III, the three populations have the three chemical composition given in Table 2, *and* three different values of helium as described below. We estimated for Populations a, b, and c, $Y = 0.246$, 0.254, and 0.275, *respectively*.

The comparison of the observed $m_X - m_{F814W}$ differences between MSa and MSc against the synthetic ones is shown in the left panel of Figure 18.

The blue squares indicate the color differences corresponding to Option I, where we assumed for the two stellar populations

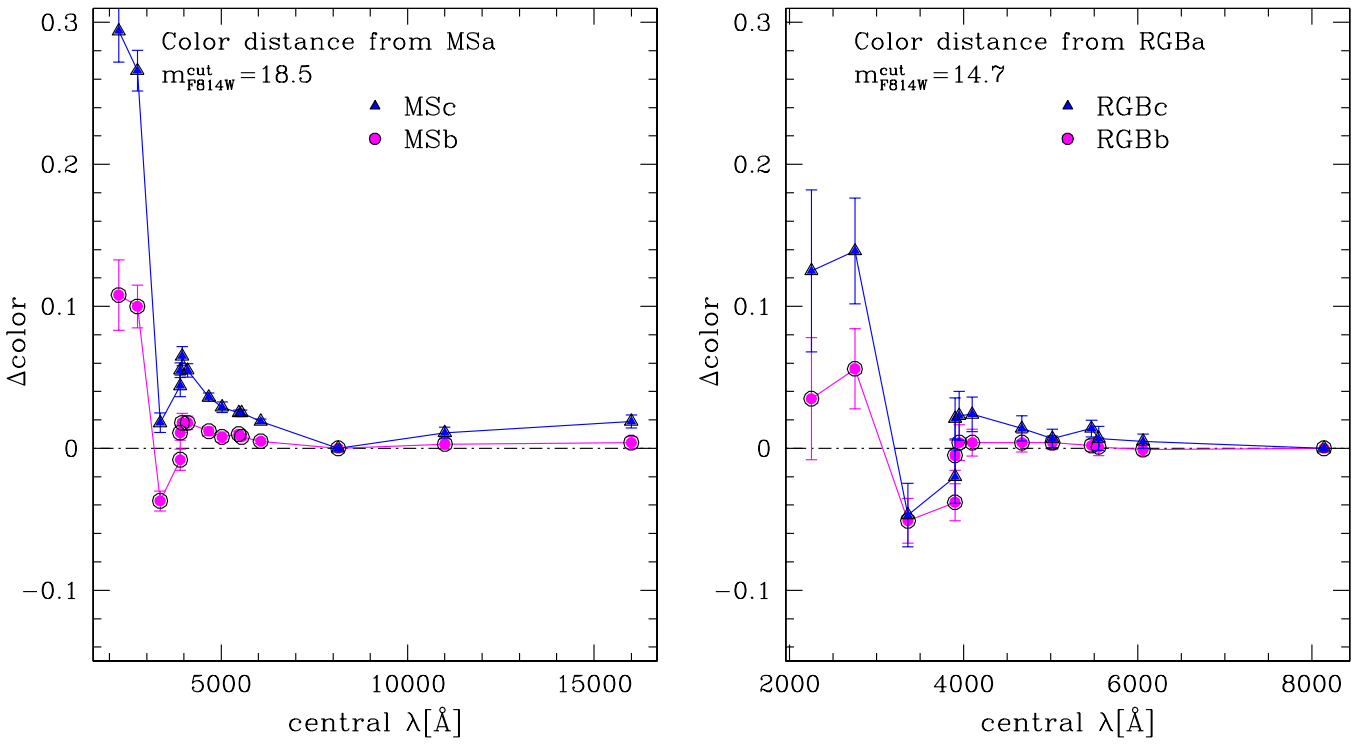

Figure 17. Left panel: $m_X - m_{F814W}$ (or $m_{F814W} - m_X$) color distance between MSb and MSa (magenta circles) and between MSc and MSa (blue triangles) as a function of the central wavelength of the X filter. Right panel: color distance between RGBb and RGBa (magenta circles) and between RGBc and the RGBa (blue triangles). The color distances of the MS and RGB sequences are measured at the reference magnitudes $m^{cut}_{F814W} = 18.5$ and $m^{cut}_{F814W} = 14.7$, respectively.

(A color version of this figure is available in the online journal.)

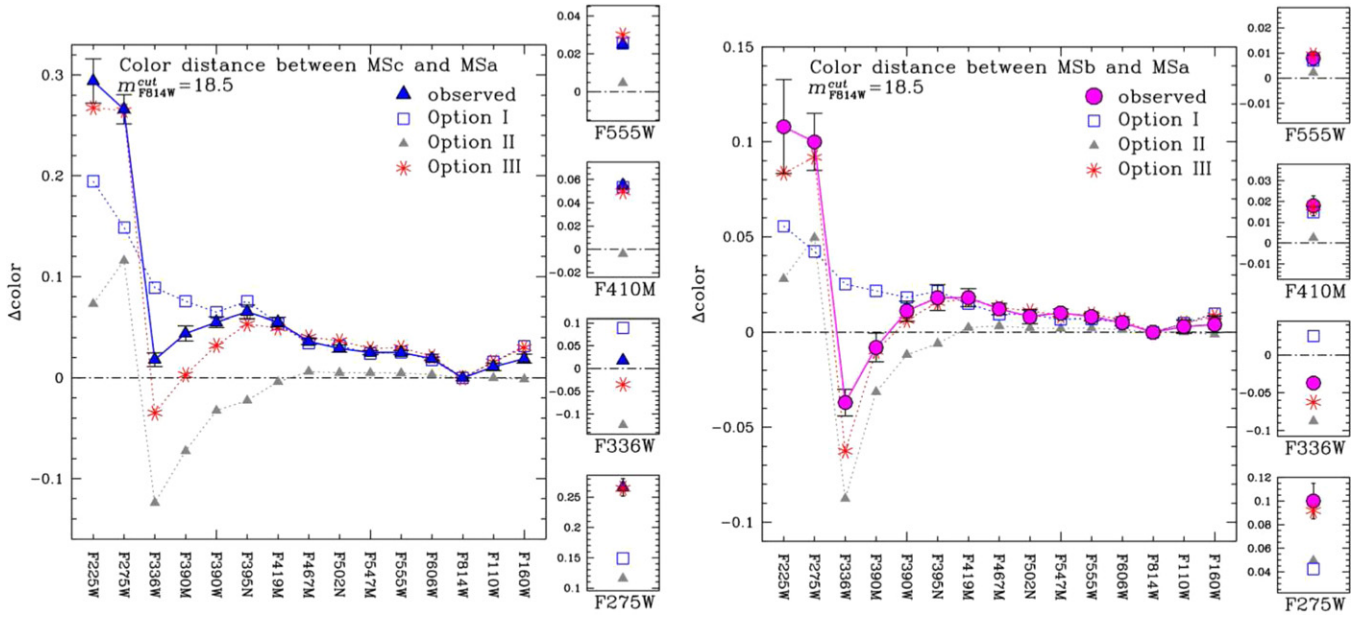

Figure 18. Color separations at different color baselines for the ridgelines of the MSc and the MSa (left), and the MSb and the MSa (right) at m_{F814W} =18.5. Observations are plotted as blue triangles and magenta circles for the MSc and the MSb, respectively, while the color differences expected from theoretical Options I, II, and III are shown as blue squares, gray triangles, and red asterisks. On the right of each panel, the small boxes correspond to regions centered on the F275W, F336W, F410M, and F555W bands.

(A color version of this figure is available in the online journal.)

the same element abundance as for MSa, but a different helium content. Similar to what observed in the cases of 47 Tuc and NGC 6397, we find a good agreement in most bands but a significant disagreement for filters bluer than ∼4000 Å, and conclude that helium cannot be the only parameter responsible for the color differences between MSa and MSc. This confirms that the observed light-element abundance of the three stellar populations plays a fundamental role in the MS morphology.

In Option II, we assumed for MSc stars the same He content as for the MSa, and the chemical composition listed in Table 3. The colors resulting from this option are represented by gray triangles in Figure 18, and indicate a significant disagreement

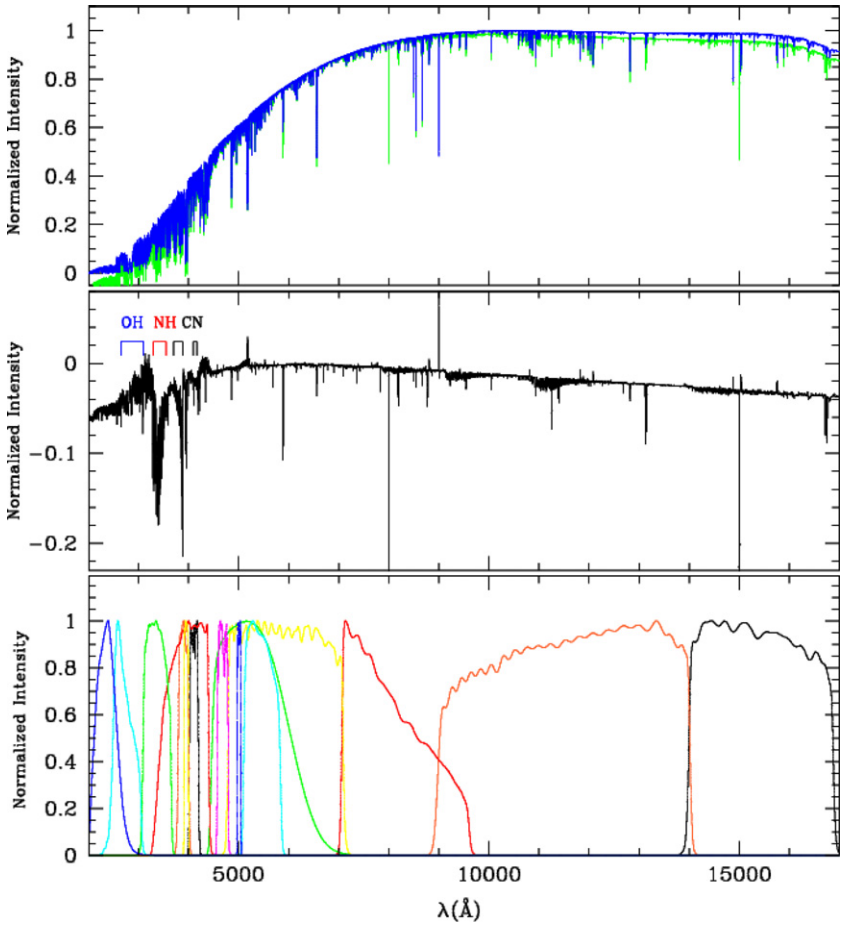

Figure 19. Upper panel: comparison of the synthetic spectra of an MSa star (green) and MSc stars (blue). Middle panel: difference between the spectra of the MSa and the MSc star. The locations of relevant molecular features are indicated. Lower panel: normalized-to-peak response of the *HST* filters used in this paper.
(A color version of this figure is available in the online journal.)

between observed and synthetic colors. It is worth noting that the observed light-element difference among the three stellar populations has a negligible effect for filters redder than ∼4000 Å as already shown by Sbordone et al. (2011).

Finally, in Option III (red asterisks), we assumed differences in both helium and chemical abundances. To determine the value of Y that best reproduces the observed points, we generated a grid of synthetic spectra by assuming different helium abundances, with Y ranging from 0.246 to 0.290 in steps of $\Delta Y = 0.001$. For each synthetic spectrum, we determined the $m_X - m_{F814W}$ color distance between MSc and MSa corresponding to each X filter, ($\Delta color_{syn}$), and calculated $d(Y) = |\Delta color_{syn} - \Delta color|$, where $\Delta color$ is the observed color distance between the two MSs in that filter.

The helium abundance (Y_*) that minimizes $d(Y)$ is assumed to be the best estimate of Y for the filter X. The helium content of MSc is then calculated as the weighted mean of the available Y_* measurements by using only those filters redder than F395N: we obtain $Y = 0.273 \pm 0.002$. The quoted error comes from the weighted mean, and does not take into account the uncertainties of the synthetic spectra or possible errors on the value we assumed for the primordial helium. Note that we have excluded from this analysis all the UV and far-UV filters as they are very sensitive to small variations of light-element abundance. Option III (red asterisks) provides the best agreement with observations, though it is not completely satisfactory at short wavelengths.

The right panel shows the comparison of the observed $m_X - m_{F814W}$ color differences between the MSa and the MSb against the synthetic one. Again, in this case, the best fit is given by Option III, and the agreement between synthetic and observed photometry is much better than what we obtained for the MSc and MSa color differences. By using the procedure described above, we obtain $Y = 0.253 \pm 0.001$ for MSb.

The synthetic spectra of an MSa and an MSc star, as calculated for Option III, are shown in the upper panel of Figure 19. The difference between the two spectra is in the middle panel, while the lower panel shows the (normalized-to-peak) bandpasses of the filters used in this paper.

In summary, the observed color differences between the three MSs are consistent with three populations with different helium and light-element abundances. Specifically, the MSa corresponds to the first stellar population with primordial He and O-rich/N-poor stars, the MSc is made of stars enhanced in He and N, but depleted in O, and MSb stars have intermediate He, C, N, and O abundances.

In Figure 20, for the three RGBs, we repeated the same analysis as performed for the MSs. We have calculated the color distance of RGBb and RGBc from RGBa at m^{cut}_{F814W} =14.7. In Figure 20, these color differences are plotted as a function of each filter and labeled with its corresponding effective wavelength.

Observations are compared with synthetic colors calculated for an RGB stars with $m^{cut}_{F814W} = 14.7$ by using the same

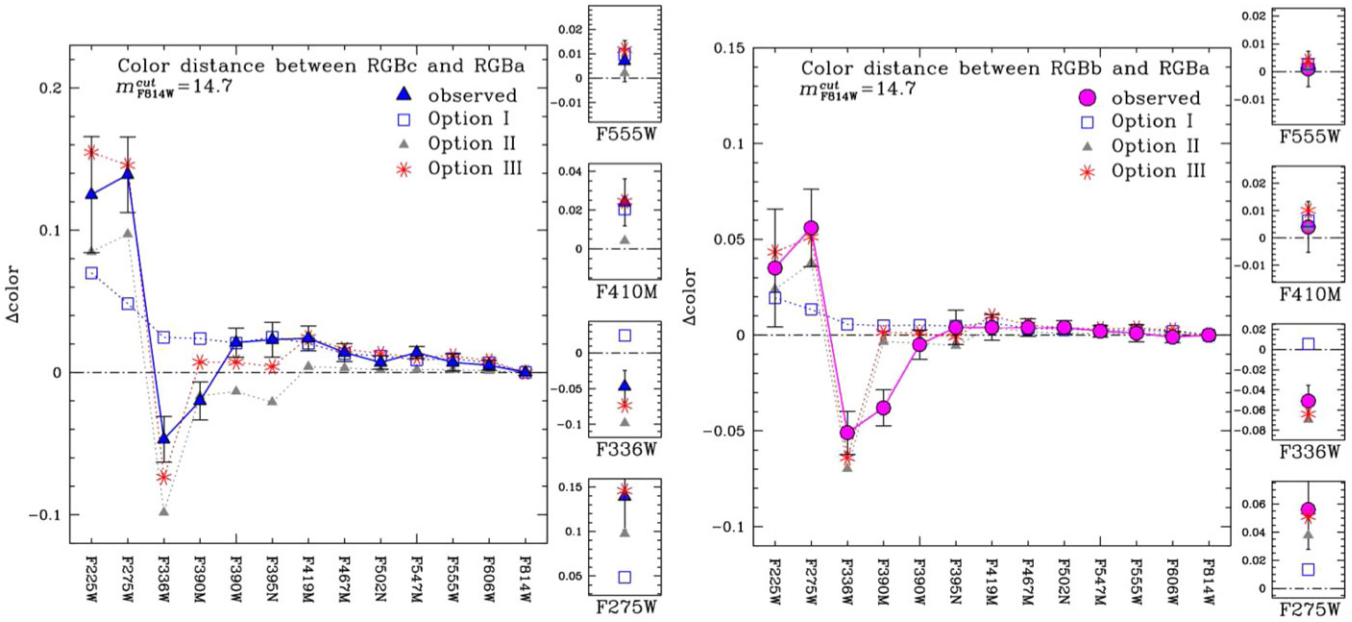

Figure 20. Left panel: $m_X - m_{F814W}$ color separation between RGBc and RGBa as a function of the central wavelength of the corresponding *X* filter. Right panel: Color separation between RGBb and RGBa. The color distances are measured at the reference magnitude $m^{cut}_{F814W} = 14.7$. Observations are plotted as blue triangles for RGc and magenta circles for RGBa, while the color differences expected from theoretical Options I, II, and III are shown as blue squares, gray triangles, and red asterisks. The small boxes correspond to regions centered on the F275W, F336W, F410M, and F555W bands.

(A color version of this figure is available in the online journal.)

procedure described for MS stars, and for the same three Options I, II, and III listed in Table 3. Similar to what was found for the MSs, the color differences between the three RGBs can be best reproduced by Option III, which reinforces the idea previously proposed that RGBa, RGBb, and RGBc stars are the progeny of MSa, MSb, and MSc stars, respectively. Specifically, by using the procedure described above for the MSs, we obtain for RGBc and RGBb helium abundances of $Y = 0.272 \pm 0.005$ and $Y = 0.255 \pm 0.004$, respectively.

6.1. The Radial Distribution of the Three Stellar Populations

In order to calculate the radial distribution of the three stellar populations in NGC 6752, we *first* divided our sample into two regions. The first one includes stars with radial distance from the cluster center smaller than 1.7 arcmin, and is covered by *HST* observations. The second one contains stars with radial distances from the center between 1.7 and 6.5 arcmin, which are included in the ground-based catalog. The upper panel of Figure 21 shows the fractions of MSa, MSb, and MSc stars with respect to the total number of MS stars as green, magenta, and blue triangles, and the fractions of RGBa, RGBb, and RGBc stars with respect to the whole RGB population as green, magenta, and blue circles.[15]

Then, we further divided the region with radial distance smaller than 1.7 arcmin into four circular subregions, each one containing almost the same number of MS stars. For each region, we calculated the fraction of MSa, MSb, and MSc stars by using the procedure already described in Section 3. Similarly, we divided the region with radial distance between 1.7 and 6.5 arcmin into two parts containing almost the same number of RGB stars, and calculated the fraction of RGBa, RGBb, and RGBc stars as in Section 5.1. The results are shown in the lower panel of Figure 21. Note that due to the relatively small number of RGB stars in the *HST* field, we preferred to limit the analysis based on *HST* data to MS stars.

The fraction of Population a, Population b, and Population c stars is listed in Table 4, where we also included the minimum and the maximum radii of the circular region (R_{min} and R_{max}), and the average radial distance of the MS or RGB stars used to estimate the populations ratio (R_{ave}). The latter is calculated as the mean radius of the MS or RGB stars in that bin.

There is no significant radial trend in the relative numbers of the three stellar populations within 6 arcmin from the cluster center. *Apparently*, these results do not support the conclusions by Kravtsov et al. (2011), who analyzed

Table 4
Fraction of Population a, Population b, and Population c Stars Calculated in Different Circular Regions with Different Radial Distance from the Cluster Center

R_{min}	R_{max}	R_{ave}	Population Ratio			Sequence
			a	b	c	
0.00	1.70	0.95	0.25 ± 0.02	0.44 ± 0.04	0.31 ± 0.03	MS
0.00	1.70	0.87	0.28 ± 0.03	0.41 ± 0.03	0.31 ± 0.03	RGB
1.70	6.13	3.26	0.27 ± 0.04	0.44 ± 0.04	0.29 ± 0.04	RGB
0.00	0.53	0.31	0.24 ± 0.02	0.47 ± 0.05	0.29 ± 0.042	MS
0.53	0.83	0.68	0.23 ± 0.02	0.52 ± 0.04	0.25 ± 0.031	MS
0.83	1.12	0.97	0.28 ± 0.02	0.42 ± 0.05	0.29 ± 0.042	MS
1.12	2.33	1.44	0.28 ± 0.03	0.44 ± 0.04	0.28 ± 0.025	MS
1.70	3.11	2.35	0.26 ± 0.05	0.45 ± 0.05	0.29 ± 0.05	RGB
3.11	6.13	4.15	0.30 ± 0.05	0.43 ± 0.05	0.27 ± 0.05	RGB

Notes. The minimum and maximum radius (R_{min} and R_{max}) of each region are listed together with the average radial distance of stars in each region (R_{ave}). The last column indicates the sequence of the CMD (MS or RGB) used to estimate the populations ratio.

[15] We note here that the fraction of stars in the different MSs has been estimated by comparing stars in small magnitude intervals (see Section 3). Since these stars have similar luminosities and the color differences between MSa, MSb, and MSc stars is quite small, incompleteness is not an issue in this comparison. In any case, the completeness level is greater than 0.67 for the adopted magnitude interval, with $m_{F814W} < 20.3$.

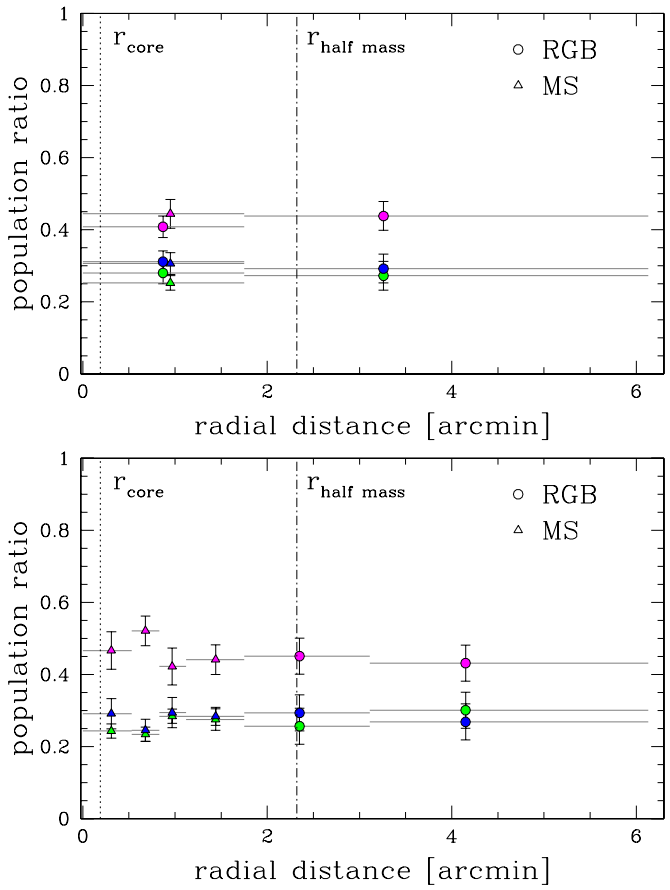

Figure 21. Radial distribution of the fraction of Population a (green symbols), Population b (magenta symbols), and Population c (blue symbols) with respect to the total number (Population a + Population b + Population c) of stars. Circles and triangles refer to the measures obtained from RGB and MS stars, respectively. The dotted and the dashed-dotted vertical lines mark the core and the half-mass radius, respectively. In the upper panel, we have used one single radial interval for *HST* and one for ground-based data. In the lower panel, we have divided the *HST* field of view into four radial bins, and the region with radial distance larger than 1.7 arcmin (ground-based data) into two bins. See text for details.

(A color version of this figure is available in the online journal.)

ground-based images and reported a strong difference in the radial distribution between the RGB subpopulations. These authors found that the change in the fraction in the two RGBs occurs at a radial distance close to the half-mass radius of the cluster ($r_h = 2.34$ arcmin; Harris 1996; updated as in 2010 December) and becomes much stronger at larger radial radii. An extension of the analysis presented in this paper to larger radial distances from the cluster center is mandatory to properly characterize the radial distributions of the different subpopulations.

As pointed out by the referee, the relaxation time of NGC 6752 at the time the secondary generations formed is a fundamental ingredient for a proper interpretation of these results. The estimate of this quantity is beyond the objectives of this paper and is complicated by the fact that NGC 6752 (as, in general, all GCs showing evidence of multiple stellar populations) may have been significantly more massive at the time of the formation of their stellar generations. (see, e.g., Conroy 2012; Goudfrooij et al. 2011; D'Ercole et al. 2010). The populations' ratio listed in Table 4 at several radial distance from the cluster center can provide useful constraints for the models of formation and evolution of stellar populations in GCs.

7. SUMMARY

We analyzed *HST* images and ground-based catalogs obtained through a large set of filters in order to identify multiple stellar populations in NGC 6752. We find that the MS of this cluster splits into three components, in close analogy with what we observed for its RGB and its SGB. We conclude that NGC 6752 hosts at least three stellar populations, whose evolution can now be followed from the MS up to the RGB tip. This result is nicely summarized in Figure 22, where we show some representative CMDs, where each population can be followed along its evolutionary phases.[16]

The multi-wavelength photometric data set allowed us to complement and extend the information on the chemical composition of the different populations available from spectroscopic chemical abundance measurements of a limited sample of stars. We calculated model atmospheres for MS and RGB stars, accounting for the available chemical composition, and demonstrated that the three groups of stars have different helium and light-element abundances. The most straightforward interpretation is that Group "a," which contains about 25% of the total number of stars, is the first stellar population, and originated in a molecular cloud with a chemical composition similar to that of the Galactic halo, of which it shares its chemical composition. The majority of stars represent a second (and third) stellar population which we named "b" (and "c") and contain about 30% (and 45%) of the cluster stars. They formed out of material that had been partly processed through first-generation stars, and are C/O-poor, N/Na/Al-rich, and enhanced in helium by $\Delta Y \sim 0.01$ and $\sim$0.03, respectively. We note that stars in each RGB sequence exhibit a wide spread in the abundance of some light elements (e.g., N and Mg), thus suggesting that the three groups of stars defined above are not chemically homogeneous. Interestingly, the HB morphology of NGC 6752 also seems to be composed of three sub-groups (Momany et al. 2002), suggesting that these three populations eventually evolve in HB stars with different properties. No radial gradient of the different stellar populations was detected within NGC 6752.

Similar conclusions have been reached for other GCs: the multiple MSs of ω Centauri and NGC 2808 suggest extreme helium abundances ($Y \sim 0.39$, e.g., Bedin et al. 2004; D'Antona et al. 2005; Piotto et al. 2007; King et al. 2012), while the multiple sequences of NGC 6397 and 47 Tuc imply small helium enhancements ($\Delta Y \sim 0.01$–0.02, Di Criscienzo et al. 2010a, 2010b; Milone et al. 2012a, 2012b). Interestingly, while in NGC 6397 and 47 Tuc there is evidence of two groups of stars with slightly different helium contents in the case of both NGC 6752 and NGC 2808, we have identified at least three stellar populations. It is worth noting that a multimodal RGB with at least three components has been also observed in NGC 6205 (Grundahl et al. 1998). A multi-band study of this cluster is mandatory to estimate the helium content of its stellar populations. Our results provide evidence that differences in helium abundance are a quite common feature of different stellar populations in GCs. D'Ercole et al. (2010, 2012) show that different combinations of helium and CNO variations can be obtained, due to the different modalities in which in each cluster the ejecta of stars are diluted with primordial gas. Further study of CMD multiple populations may allow us to constrain for each cluster the parameters necessary to its specific model.

[16] The fiducial lines of the three stellar populations are available at this url: http://www.astro.unipd.it/globulars/.

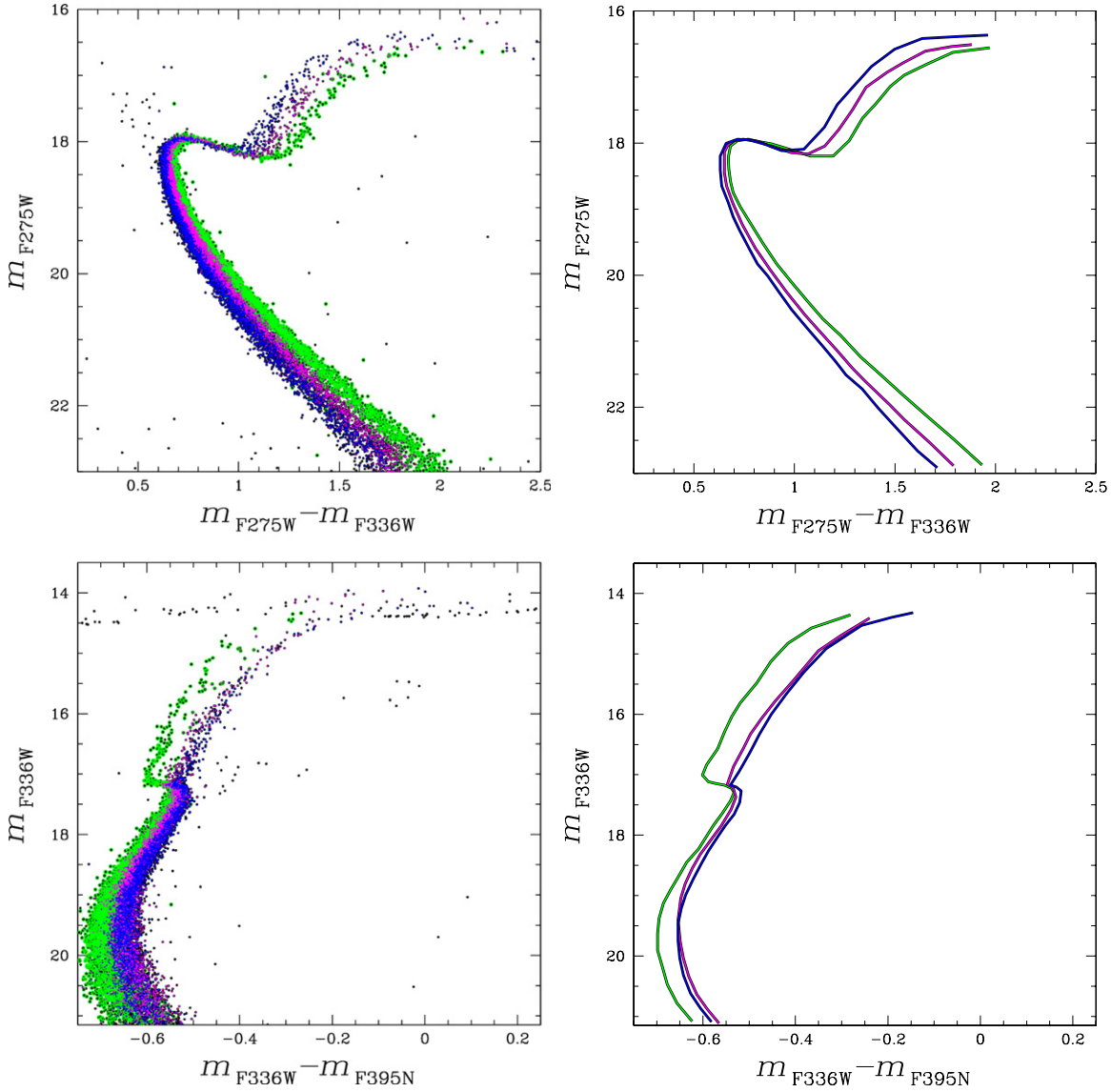

Figure 22. m_{F275W} versus $m_{F275W} - m_{F336W}$ (top) and m_{F336W} versus $m_{F336W} - m_{F395N}$ CMDs. We have colored green, magenta, and blue the three groups of stars selected in Figures 5, 10, and 12. The fiducial lines of the three stellar populations of NGC 6752 are shown on the right.

(A color version of this figure is available in the online journal.)

Finally, we discuss a potential disagreement between spectroscopic and photometric evidence of multiple stellar populations in GCs that needs to be solved for further progress in our understanding of GC stellar populations.

We are grateful to the referee for many useful suggestions that significantly improved the quality of the manuscript. Support for this work has been provided by the IAC (grant 310394), and the Education and Science Ministry of Spain (grants AYA2007-3E3506, and AYA2010-16717). A.P.M. acknowledges the financial support from the Australian Research Council through Discovery Project grant DP120100475. A.B., S.C., and G.P. acknowledge partial support by the ASI-INAF I/009/10/0 grant, and PRIN-INAF 2010. G.P. acknowledges partial support by the Universita' di Padova CPDA101477 grant.

REFERENCES

Anderson, A. J. 1997, Ph.D. thesis, Univ. California, Berkeley
Anderson, J., Bedin, L. R., Piotto, G., Yadav, R. S., & Bellini, A. 2006, A&A, 454, 1029
Anderson, J., & King, I. R. 2006, Instrument Science Report ACS 2006-01, 34 pages, 1
Anderson, J., Piotto, G., King, I. R., Bedin, L. R., & Guhathakurta, P. 2009, ApJL, 697, L58
Anderson, J., Sarajedini, A., Bedin, L. R., et al. 2008, AJ, 135, 2055
Bedin, L. R., Cassisi, S., Castelli, F., et al. 2005, MNRAS, 357, 1038
Bedin, L. R., Piotto, G., Anderson, J., et al. 2004, ApJL, 605, L125
Bellini, A., Anderson, J., & Bedin, L. R. 2011, PASP, 123, 622
Bellini, A., & Bedin, L. R. 2009, PASP, 121, 1419
Bellini, A., Bedin, L. R., Piotto, G., et al. 2010, AJ, 140, 631
Bellini, A., Piotto, G., Milone, A. P., et al. 2013, ApJ, 765, 32
Briley, M. M. 1997, AJ, 114, 1051
Briley, M. M., Hesser, J. E., Bell, R. A., Bolte, M., & Smith, G. H. 1994, AJ, 108, 2183
Busso, G., Cassisi, S., Piotto, G., et al. 2007, A&A, 474, 105
Cannon, R. D., Croke, B. F. W., Bell, R. A., Hesser, J. E., & Stathakis, R. A. 1998, MNRAS, 298, 601
Carretta, E., Bragaglia, A., Gratton, R. G., et al. 2009, A&A, 505, 117
Carretta, E., Bragaglia, A., Gratton, R. G., et al. 2010, A&A, 516, A55
Carretta, E., Bragaglia, A., Gratton, R., D'Orazi D'Orazi, V., & Lucatello, S. 2011, A&A, 535, A121
Carretta, E., Bragaglia, A., Gratton, R. G., Lucatello, S., & D'Orazi, V. 2012, ApJL, 750, L14

Carretta, E., Bragaglia, A., Gratton, R. G., Lucatello, S., & Momany, Y. 2007, A&A, 464, 927
Carretta, E., Gratton, R. G., Lucatello, S., Bragaglia, A., & Bonifacio, P. 2005, A&A, 433, 597
Cassisi, S., Salaris, M., Anderson, J., et al. 2009, ApJ, 702, 1530
Castelli, F. 2005, MSAIS, 8, 25
Catelan, M., Valcarce, A. A. R., & Sweigart, A. V. 2010, in IAU Symp. 266, Star Clusters: Basic Galactic Building Blocks Throughout Time and Space, ed. R. de Grijs & J. R. D. Lepine (Cambridge: Cambridge Univ. Press), 281
Conroy, C. 2012, ApJ, 758, 21
Conroy, C., & van Dokkum, P. G. 2012, ApJ, 760, 71
Cottrell, P. L., & Da Costa, G. S. 1981, ApJL, 245, L79
Dalessandro, E., Salaris, M., Ferraro, F. R., et al. 2011, MNRAS, 410, 694
D'Antona, F., Bellazzini, M., Caloi, V., et al. 2005, ApJ, 631, 868
D'Antona, F., & Caloi, V. 2004, ApJ, 611, 871
D'Antona, F., & Caloi, V. 2008, MNRAS, 390, 693
D'Antona, F., Caloi, V., Montalbán, J., Ventura, P., & Gratton, R. 2002, A&A, 395, 69
Denisenkov, P. A., & Denisenkova, S. N. 1989, ATsir, 1538, 11
D'Ercole, A., D'Antona, F., Carini, R., Vesperini, E., & Ventura, P. 2012, MNRAS, 423, 1521
D'Ercole, A., D'Antona, F., Ventura, P., Vesperini, E., & McMillan, S. L. W. 2010, MNRAS, 407, 854
di Criscienzo, M., D'Antona, F., & Ventura, P. 2010a, A&A, 511, A70
di Criscienzo, M., Ventura, P., D'Antona, F., Milone, A., & Piotto, G. 2010b, MNRAS, 408, 999
Goudfrooij, P., Puzia, T. H., Chandar, R., & Kozhurina-Platais, V. 2011, ApJ, 737, 4
Gratton, R., Sneden, C., & Carretta, E. 2004, ARA&A, 42, 385
Gratton, R. G., Bonifacio, P., Bragaglia, A., et al. 2001, A&A, 369, 87
Gratton, R. G., Lucatello, S., Carretta, E., et al. 2011, A&A, 534, A123
Grundahl, F., Briley, M., Nissen, P. E., & Feltzing, S. 2002, A&A, 385, L14
Grundahl, F., Vandenberg, D. A., & Andersen, M. I. 1998, ApJL, 500, L179
Grundahl, F., Vandenberg, D. A., Stetson, P. B., Andersen, M. I., & Briley, M. 2000, in Proc. 35th Liege International Astrophysical Colloquia, The Galactic Halo: from Globular Cluster to Field Stars, ed. A. Noels, P. Magain, D. Caro et al. (Liege, Belgium: Institut d'Astrophysique et de Geophysique), 503
Harris, W. E. 1996, AJ, 112, 1487 (December 2010 update)
King, I. R., Bedin, L. R., Cassisi, S., et al. 2012, AJ, 144, 5
Kraft, R. P. 1979, ARA&A, 17, 309
Kraft, R. P. 1994, PASP, 106, 553
Kraft, R. P., Sneden, C., Langer, G. E., & Prosser, C. F. 1992, AJ, 104, 645
Kravtsov, V., Alcaíno, G., Marconi, G., & Alvarado, F. 2011, A&A, 527, L9
Kurucz, R. L. 2005, MSAIS, 8, 14
Lee, J.-W., Kang, Y.-W., Lee, J., & Lee, Y.-W. 2009, Natur, 462, 480
Lind, K., Charbonnel, C., Decressin, T., et al. 2011, A&A, 527, A148
Marino, A. F., Milone, A. P., Sneden, C., et al. 2012, A&A, 541, A15
Marino, A. F., Villanova, S., Milone, A. P., et al. 2011, ApJL, 730, L16
Marino, A. F., Villanova, S., Piotto, G., et al. 2008, A&A, 490, 625
Milone, A. P., Bedin, L. R., Piotto, G., & Anderson, J. 2009, A&A, 497, 755
Milone, A. P., Bedin, L. R., Piotto, G., et al. 2008, ApJ, 673, 241
Milone, A. P., Marino, A. F., Cassisi, S., et al. 2012a, ApJL, 754, L34
Milone, A. P., Marino, A. F., Piotto, G., et al. 2012b, ApJ, 745, 27
Milone, A. P., Piotto, G., Bedin, L. R., et al. 2012c, ApJ, 744, 58
Milone, A. P., Piotto, G., Bedin, L. R., et al. 2012d, A&A, 540, A16
Milone, A. P., Piotto, G., King, I. R., et al. 2010, ApJ, 709, 1183
Momany, Y., Bedin, L. R., Cassisi, S., et al. 2004, A&A, 420, 605
Momany, Y., Piotto, G., Recio-Blanco, A., et al. 2002, ApJL, 576, L65
Norris, J. 1981, ApJ, 248, 177
Norris, J. E. 2004, ApJL, 612, L25
Norris, J., Cottrell, P. L., Freeman, K. C., & Da Costa, G. S. 1981, ApJ, 244, 205
Norris, J., & Freeman, K. C. 1979, ApJL, 230, L179
Pietrinferni, A., Cassisi, S., Salaris, M., & Castelli, F. 2004, ApJ, 612, 168
Pietrinferni, A., Cassisi, S., Salaris, M., Percival, S., & Ferguson, J. W. 2009, ApJ, 697, 275
Piotto, G., Bedin, L. R., Anderson, J., et al. 2007, ApJL, 661, L53
Piotto, G., Milone, A. P., Anderson, J., et al. 2012, ApJ, 760, 23
Piotto, G., Villanova, S., Bedin, L. R., et al. 2005, ApJ, 621, 777
Ramírez, S. V., & Cohen, J. G. 2002, AJ, 123, 3277
Sarajedini, A., Bedin, L. R., Chaboyer, B., et al. 2007, AJ, 133, 1658
Sbordone, L., Bonifacio, P., & Castelli, F. 2007, in IAU Symp. 239, Convection in Astrophysics, ed. F. Kupka, I. Roxburgh, & K. Chan (Cambridge: Cambridge Univ. Press), 71
Sbordone, L., Salaris, M., Weiss, A., & Cassisi, S. 2011, A&A, 534, A9
Smith, G. H., & Norris, J. E. 1993, AJ, 105, 173
Sneden, C., Kraft, R. P., Langer, G. E., Prosser, C. F., & Shetrone, M. D. 1994, AJ, 107, 1773
Stetson, P. B. 2005, PASP, 117, 563
Villanova, S., Piotto, G., & Gratton, R. G. 2009, A&A, 499, 755
Yong, D., Grundahl, F., Johnson, J. A., & Asplund, M. 2008, ApJ, 684, 1159
Yong, D., Grundahl, F., Lambert, D. L., Nissen, P. E., & Shetrone, M. D. 2003, A&A, 402, 985
Yong, D., Grundahl, F., Nissen, P. E., Jensen, H. R., & Lambert, D. L. 2005, A&A, 438, 875